2014

Delft University of Technology

Christiaan Roose

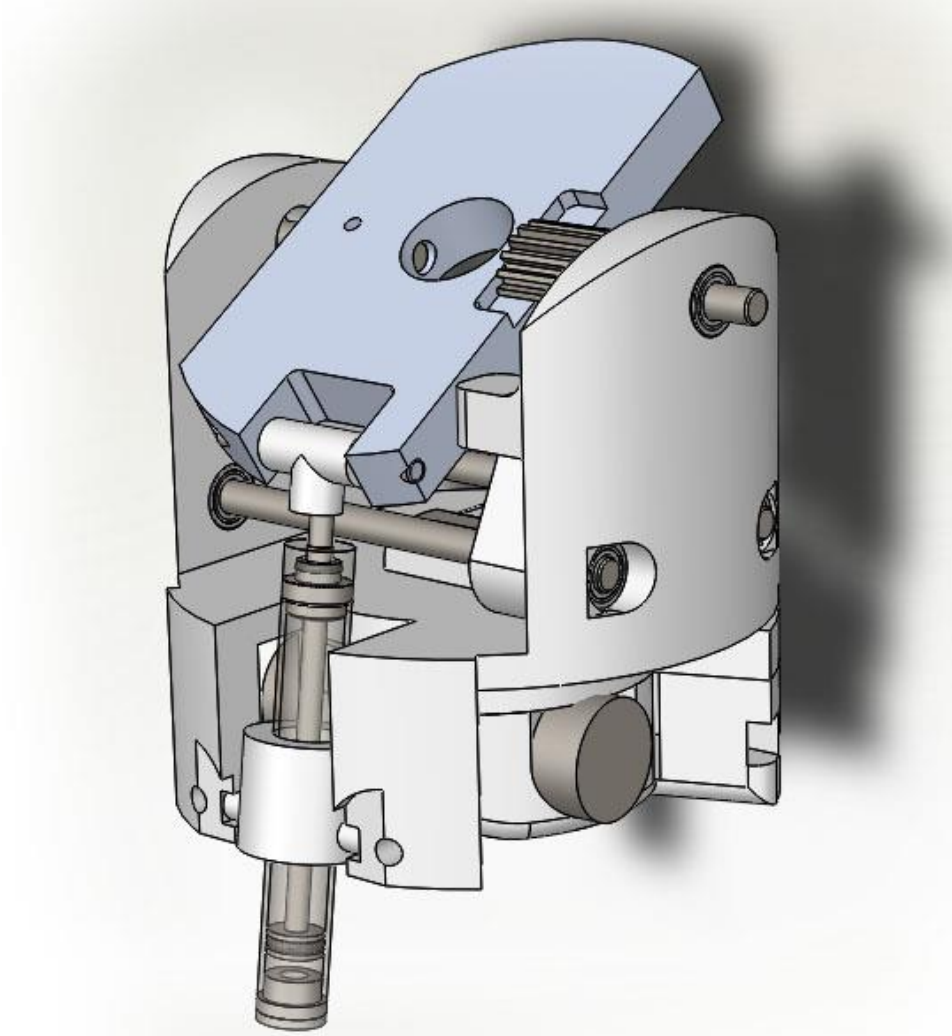

[TWO-DEGREE-OF-FREEDOM PNEUMATICALLY POWERED WRIST PROSTHESIS]

The vast developments in the electronic industry over the past few decades have provided smaller and lighter electrical components that spurred advances in dexterous upper extremity prostheses. Prosthetic companies have commercialized anthropomorphic artificial hands including over 10 different grasp patterns and auto grasp features to prevent objects slipping. However, wrist function remains inadequate. This forces prosthetic users to compensate for lack of wrist function, causing musculoskeletal pain in the neck/upper back, shoulders, and the residual arm. Adding a multiple degree of freedom wrist to the already overweight hand prostheses forces research in alternative actuation methods. Considering these issues and the fact that past studies have shown pneumatic actuation to be a promising lightweight option to actuate upper extremity prostheses, the goal of this research is to develop a functional lightweight pneumatically powered two-degree-of-freedom wrist prosthesis. The developed prototype is designed to actively move the wrist in a certain position where it will passively lock in place in order to be able to perform the desired task. With a weight of 95.4 grams and a with a circumference similar to the average human wrist, the final prototype enables enough output torque to employ a 500 gram prosthetic hand over a maximum range of motion of 42°/42° for flexion/extension and 51°/52° for pro-/supination. In its current form, however, significant improvements can be made by optimization of material choice in order to reduce friction, reduce weight, and increase the amount of torque the locking mechanism can withstand. All things considered, this prototype reveals that pneumatically actuated prostheses show promise of becoming a true lightweight competitor for the current industry standard in upper extremity powered prosthetics.

TABLE OF CONTENTS

LIST OF FIGURES

LIST OF TABLES

1 INTRODUCTION

Individuals living with an incurable disease or disorder find themselves having to adjust their lifestyles to cope with the symptoms and effects of their condition. For amputees in particular, the consequences are very apparent and have a huge impact on their Activities of Daily Living (ADL).

In the case of upper extremity amputations, the leading cause for this procedure is trauma, followed by cancer and congenital disorders [1]. When caused by trauma (work accidents, road traffic accidents, violence, frostbite, etc.), patients are forced to change their lifestyle from one moment to the next which not only impairs them functionally, but also forces an immediate change of self-image and social interaction [2]. These abrupt changes can have a huge impact on a patient's psychological well-being and they are known to cause significant depressive and/or anxiety symptoms in about 30% of patients [3]. So although we can only observe a relatively low incidence rate for traumatic upper extremity amputations per year (on average 42 cases per year in The Netherlands, 2001-2005 [4]), the large impact on the quality of life of these patients calls for further research in the development of new technologies to give back to these patients their independence, physical functionality, and self-confidence.

With this goal in mind, a large number of upper extremity prostheses have already been developed, ranging from passive arm prostheses (mainly used for cosmetic purposes) towards highly advanced controllable prostheses [5] [6] [7]. However, there is no such thing as a perfect prosthesis. In fact, many factors influence the use and rejection of prostheses given to patients. It is stated that the core causes of rejection are inadequate information of the patient, incompetent professionals, and inadequate equipment [8]. The first two arguments here are a matter of educating the professionals (i.e. physicians, occupational therapists, etc.) on how to properly inform/train the patient, and how to, for example, adequately dimension the size of the socket. Unlike these procedural improvements for amputee rehabilitation, solving the problem of inadequate equipment will require great technological advances in prosthetics to solve the three most important reasons for rejection among amputees; prosthetic comfort, function, and control [9].

Although the most recent products from the major artificial hand manufacturers are equipped with technical highlights (such as auto-grasp features, custom gesture selection, etc.) [5] [6] [7], modern upper myoelectric hand prostheses only partly fulfill the requirements from a user-centered perspective [10]. For a typical below elbow myoelectric prosthesis, the user contracts the flexor or extensor muscles on the forearm to control a desired joint and uses mode switching techniques, such as co-contractions, to switch between the different pre-programmed joints [11]. Much progress is being made, nowadays, in the development of implantable peripheral nerve cuff electrodes [12], cortical implants [13], and EMG pattern recognition [14] to increase the amount of available inputs to the system, potentially providing even more functionality, or even the option to control multiple joints simultaneously. Obviously, all these functions will require more and more actuators, which will inadvertently increase the weight of the device. Concurrently, consumer preference studies have shown that reducing the weight is in fact the highest priority for users of upper extremity prostheses [15].

Along with this desired reduction in prosthetic mass, increased wrist function is also prominently in the top three of research demands from patients [15]. It can be imagined that users will have to compensate for this lack of wrist function by putting themselves in a variety of awkward upper body positions; these movements are known as compensatory movements. A recent Norwegian study among a large number of prosthetic users revealed that lack of wrist function has indeed been proven to cause users to be prone to injury in the upper back, neck,

and the residual limb due to prolonged use of compensatory movements [16]. Also, these patients were diagnosed 24% more often with musculoskeletal overuse syndromes than healthy controls. There is, in fact, an increasing number of studies analyzing the cause, nature and results of these compensatory movements in upper extremity prosthesis users [17] [18] [19] [20]. All of which conclude with a recommendation for improved wrist function.

Problem: *Current upper extremity prostheses provide inadequate wrist function, leading to mental and physical problems in prosthetic users.*

As of now, there is still no powered wrist commercially available that provides wrist functions other than rotation. In fact, even the choice for these single degree-of-freedom (DoF) rotators is very limited for consumers; there is the VASI Wrist Rotator (100 grams, *LTI / Liberating Technologies, Inc.*) [21], the MC Wrist Rotator (143 grams, *Motion Control, Inc.*) [22], and the Electric Wrist Rotator 10S17 (96 grams, *Otto Bock*) [23]. Other than those, only two experimental 2-DoF wrist prototypes have been developed for trans-radial amputees; the UNB Wrist (200 grams) [24], and the Fourier Designs Wrist (454 grams) [25]. Both of which stated that the weight of the prototypes will need to be reduced further in the future.

So, increasing the functionality of a prosthetic wrist seems to contradict the demand for large weight reductions of the product. Or does it? A literature study on the design considerations regarding the development of a multiple-DoF prosthetic wrist [26] preceding this report concluded that pneumatic actuation is a more than viable short term actuation method to achieve both.

Goal: *The goal of this project is to develop a functional lightweight pneumatically powered two-degree-of-freedom wrist prosthesis.*

Section *2 Background* will start with an overview of the basic pneumatic principles that were used during the development of the wrist prototype. This is followed by Section *3 Methods and Materials* in which the design requirements are drawn up, the cylinder parameter optimization process is explained, the material choices are described, and the final prototype is presented per elementary component in this design; the rotation mechanism, the flexion/extension mechanism, and the locking mechanism. Finally, Section *4 Test* Results will show whether or not the design requirements for the prosthetic wrist prototype have been met.

2 BACKGROUND

Looking into pneumatic actuation as a way to control powered prostheses originates from the demand for large weight reductions in prosthetics, while evermore increasing functionality. Long before Soviet scientists were the first to use transistors in a prosthetic hand [27], pneumatic actuation was the only viable way to actuate a powered prosthesis. In fact, the first externally powered upper extremity prosthesis in 1877 was powered by operating a bellow between the upper arm and the torso [28]. Later, the first compressed air actuated prosthesis was realized in 1915 [29] which for the first time no longer required any energy supplied by the user to operate. Pneumatic actuation remained the dominant actuation method worldwide up until the 1970's, when body-powered and myoelectric systems became the industry standard. The reason for this is that canisters of gas were expensive, had low energy storage densities, and were difficult to distribute [30]. Nowadays, researchers are again trying to exploit the advantageous light weight, low sound emission, and natural compliance properties of pneumatic actuation. In order to optimally make use of the power supply (i.e. compressed gas container), some knowledge is required of pneumatic systems.

Very similar to optimizing electrical prosthetic systems to ensure a satisfactory battery life, it is important to optimize a pneumatically powered prosthetic system such that the compressed gas containers only rarely need to be replaced. In other words, the amount of gas used with respect to the generated torque should be as little as possible per intended motion of the user.

The first parameter in the optimization process is to select the most appropriate type of gas to use for this application. Compressed carbon dioxide (CO_2) is considered to be the most viable option due to its colorless, odorless, non-flammable, and non-toxic nature (in low concentrations). Moreover, its physical property of liquefying at room temperature at relatively low pressures (5.1 MPa.) makes it an exceptionally viable gas to safely store large quantities in small containers [31]. Being a common byproduct in industrial processes and its popularity in commercial applications make for a very cheap and globally available pneumatic power supply. The smallest regular commercial CO_2 cartridges can be purchased easily with properties similar to the values found in Table 1 [32].

TABLE 1, PROPERTIES OF A REGULAR COMMERCIAL CO_2 CANISTER

MOSA® CO_2 Charger	
material	steel
dimensions	Ø 17.8 x 66.0 mm.
cartridge mass	28 g
contents	8g CO_2 at 5.7 MPa (20 °C)

Secondly, the optimal operating pressure should be determined. Pressure is defined as force per area. When gas molecules collide with the sides of a container, they are exerting a force over the area of that container. This concept is used in pneumatics to increase the pressure (i.e. molecular collision forces over the area of the cylinder head) until all external forces are overcome and motion of the cylinder rod is realized. Using the pressurized CO_2 canister from Table 1 requires the use of a pressure reducing valve connected directly to the nozzle of the canister in order to reduce the pressure to a level at which the prosthetic wrist will function at the lowest possible gas expenditure. Which parameters determine this particular supply pressure? The following subsection will discuss the parameters taken into account when establishing the ideal supply pressure.

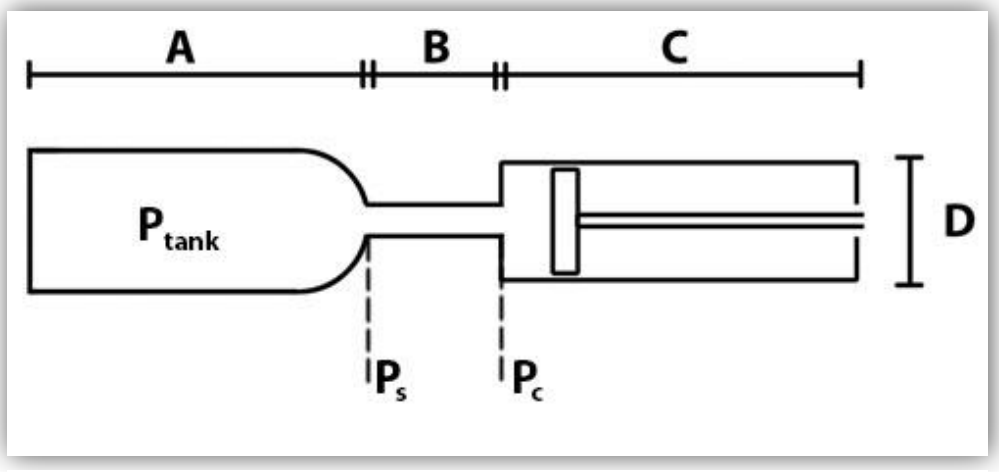

FIGURE 1. A SCHEMATIC OVERVIEW OF THE SYSTEM THAT WILL BE USED TO POWER THE PROSTHESIS. PRESSURIZED GAS FLOWS FROM THE CONTAINER (A) THROUGH THE DUCT (B) INTO THE CYLINDER (C). A PRESSURE REDUCING VALVE WILL REDUCE THE PRESSURE IN THE CONTAINER (P_{TANK}) TO THE OPTIMAL SUPPLY PRESSURE (P_S) AFTER WHICH IT DROPS TO THE CYLINDER PRESSURE (P_C) DUE TO FRICTIONAL LOSSES IN THE DUCT. THE DIAMETER OF THE CYLINDER (D) CAN THEN BE USED TO DETERMINE THE OUTPUT FORCE OF THE CYLINDER WITH RESPECT TO THE AMOUNT OF GAS CONSUMED PER CYLINDER STROKE.

Figure 1 gives a schematic overview of the pressurized CO_2 cartridge (A), the connecting tubing (B), and the cylinder (C). The supply pressure (P_s) is defined as the gas leaving the pressure reducing valve at the junction between the CO_2 canister (A) and the pneumatic tubing (B). Traveling through the tubing, the pressure will drop until it reaches the cylinder pressure (P_c) at the junction between the tubing (B) and the cylinder (C). The pressure loss in the tube is modeled according to the momentum equation of compressible duct flow with friction [33].

With this approximation of P_c, one can estimate the output force of the cylinder rod using the diameter of the cylinder (D). Estimating the amount of gas consumed from the CO_2 container (in grams) per stroke of the cylinder will determine the parameters of the pneumatic system that maximize the amount of output force while minimizing the amount of gas consumed per stroke. At these conditions, however, modeling the CO_2 as a real gas (non-ideal) is imperative to receive accurate results. Nonlinearities in the molecular behavior of the gas at high pressures cause nonlinear behavior in the amount of gas used per stroke over the range of different cylinder pressures. The two most significant effects are listed below.

- The amount of space that the gas molecules take up in the volume of the cylinder no longer becomes negligible at high pressures. This is a favorable effect for this specific application because it allows for using less CO_2 to achieve the same amount of output force.
- The mutual attraction between the CO_2 molecules no longer becomes negligible at high pressures. This will have a negative effect for this specific application because the closely compacted molecules now significantly attract each other, causing them to slow down before they collide with the wall of the cylinder head.

With these nonlinear effects modeled into the behavior of the cylinder, an optimum can be found at the pressure of which the amount of gas consumed per stroke is minimized. Adding up the frictional pressure loss over the duct flow will give the optimal supply pressure P_s. A study in which a prototype was created of a pneumatically powered children's upper extremity

prosthesis estimated the optimal supply pressure for the same duct-cylinder system to be 1.2 MPa [34]. Due to the similarity of that system with the design of this pneumatically powered wrist, it is decided to set the value for the pressure reducing valve to the same 1.2 MPa for the design of this wrist prototype.

3 METHODS AND MATERIALS

The following will elaborate on the starting point of the design in subsection *3.1 Design Requirements*, the various fundamental steps that were taken that shaped the design in *3.2 Parameter Optimization*, and the chosen materials in subsection *3.3 Materials* in order to come to the final design reported in *3.4 Design*.

3.1 DESIGN REQUIREMENTS

It is of the utmost importance to fully appreciate and understand the design priorities from a user point of view in order to prevent excessive prosthesis rejection. The requirements are based on a user centered approach which is generally applicable to all novel prosthetic designs; the WILMER approach [8]. In this method, user demands are subdivided into cosmesis, comfort, and control.

Cosmetics; a study among 2847 amputees revealed the magnitude of the importance of aesthetic hand prostheses [2]. The authors of that study conclude that aesthetics in prostheses play an important therapeutic role towards acceptance and recovery in amputation. Furthermore, a study among individuals with upper limb loss revealed that according to prosthetic users one of the top research priorities in body powered and electric prosthesis should be to draw “less visual attention” [35]. During the design of a prosthetic wrist, it is therefore important that the prosthetic wrist resembles the shape of a human wrist (average wrist circumference: 165.9±7.10 mm [36]), and a realistically looking cover (e.g. silicone glove) should be provided [2]. Also, it is advised to avoid sharp edges and pollutants (oil, grease, etc.) in order to increase the cosmetic value [8].

Comfort; it must be understood that the interface between the residual limb and the socket, no matter how, creates a microenvironment that is unfamiliar to the natural protection mechanisms of the skin. Sweating into the socket can result in a change of fit, which in turn results in increased shear forces that damage the skin. Furthermore, excessive sweating eventually leads to maceration (i.e. softening and whitening of wet skin) which creates a vulnerability for fungal or bacterial infections [37]. Although the interface between the socket and the skin is not directly a concern when designing a prosthetic wrist, there are definitely factors that influence this microenvironment indirectly. The primary factor of concern is weight; a lightweight construction of the prosthesis will decrease gravity imposed shear forces on the skin [8]. However, no maximum weight guidelines have yet been established in literature. As users are already unsatisfied with the weight of current devices [15], the weight for a novel wrist should not exceed current commercial products (approx. 100 grams [21] [22] [23]). Also, actuators involved in wrist control may cause local temperature fluctuations during operation. It must be ensured that these changes in temperature do not increase the likelihood of sweating, regarding the aforementioned risks.

Control; for prosthetic control, a list of goals has been made that should serve as a guideline in artificial arm, wrist, and hand design [38].

1. *Low mental loading or subconscious control.*
2. *User friendly or simple to learn to use.*
3. *Independence in multifunctional control.*
4. *Simultaneous coordinated control of multiple functions (parallel control).*
5. *Direct access and instantaneous response (speed of response).*
6. *No sacrifice of human functional ability*
7. *Natural appearance.*

Much research is still needed for all seven requirements to be fully operational in any upper extremity prosthesis, however, research in neural prosthetics [39] and EMG pattern recognition [14] is advancing gradually towards realizing the first four guidelines described above. In an attempt to converge the mechanical design of an artificial wrist with these recent advances in prosthetic control, it is important to mechanically facilitate the possibility of independent and simultaneous control as proposed in guidelines three and four. The mechanical design of an artificial wrist should therefore ideally be able to control the two most important degrees-of-freedom (DoF) of a healthy human wrist (rotation and flexion/extension), while also being able to operate these DoFs simultaneously and independently from each other (i.e. one actuator per DoF). Research shows that in order to successfully perform the vast majority of activities of daily living, a range of motion of 40°/40° flexion/extension [40] and 50°/50° pro-/supination [41] will suffice. The fifth attribute regards the time delays that the mechanical design and/or the actuators introduce into the system. Response of the prosthetic wrist must be immediate or users will have a hard time to perform basic tasks and will have trouble learning to cope with this delay (both interfering with guidelines one and two and therefore increasing the likelihood of rejection of the prosthesis). The sixth guideline speaks for itself; a prosthetic product must always add, not subtract to user function. Finally, the seventh guideline (natural appearance; not identical to aesthetics) indicates that care must be taken in the design of the mechanical system and during the selection of the actuators that motions of the wrist will be smooth and do not appear mechanical as this may draw too much unwanted attention in social situations.

Based on the aforementioned ranges of motion of rotation and flexion/extension, it is possible to deduct the final design requirement; required torque. It is assumed that the wrist will primarily be used to move the hand in a desired position after which the power supply is cut off and the system locks in place. The torque requirement is therefore based on the ability to overcome the gravitational forces of the prosthetic hand with the largest possible moment arms of the configuration as shown in Figure 2. The mass of the prosthetic hand is an assumed 500 grams (assumption based on the most common guideline for prosthetic hand design found in literature [42]) with an assumed center of mass of 61 mm from the center of rotation (assumption based on healthy human hand [43]). This results in a minimum required torque of 200 N·mm for rotation and 300 N·mm for flexion/extension.

- Rotation
  - $0.500\ [kg] \cdot 61.0\ [mm] \cdot \sin(40°) \cdot 9.81\ [N/kg] = \sim 200\ [N \cdot mm]$
- Flexion/extension
  - $0.500\ [kg] \cdot 61.0\ [mm] \cdot 9.81\ [N/kg] = \sim 300\ [N \cdot mm]$

In order for the system to lock in place, the locking mechanism in the wrist should withstand at the very least the same gravitational forces described above. Since no minimum wrist torque requirements for ADLs are known in literature, the locking requirements will feature the same 200 N·mm and 300 N·mm as a bare minimum for flexion/extension and rotation respectively.

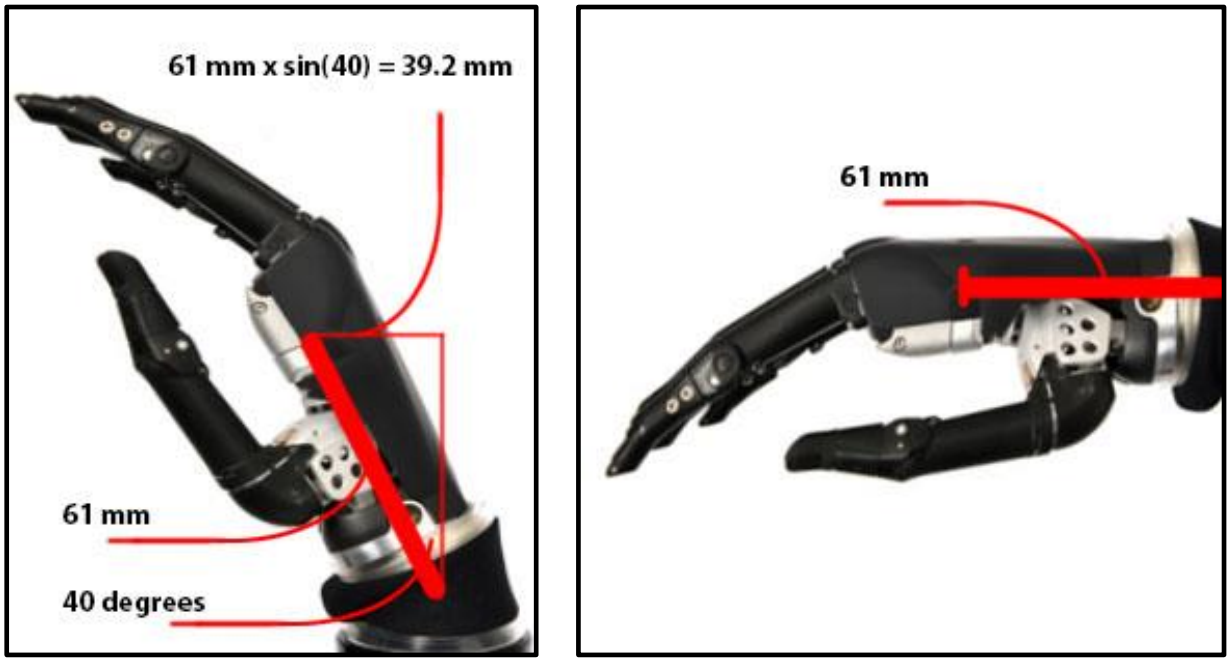

FIGURE 2. REPRESENTATION OF THE MOMENT ARMS CONCERNING THE ESTIMATION OF THE MAXIMUM REQUIRED TORQUE. ON THE LEFT; THE LARGEST POSSIBLE MOMENT ARM FOR ROTATION IS SHOWN USING THE CENTER OF MASS OF A HEALTHY HUMAN HAND [43] AND THE MAXIMUM NEEDED AMOUNT OF FLEXION FOR ACTIVITIES OF DAILY LIVING [40]. ON THE RIGHT; THE LARGEST POSSIBLE MOMENT ARM FOR FLEXION/EXTENSION. THIS RESULTS IN A REQUIRED MAXIMUM TORQUE OF APPROXIMATELY 200 N·MM FOR ROTATION AND 300 N·MM FOR FLEXION/EXTENSION.

TABLE 2. SUMMARY OF THE DESIGN REQUIREMENTS FOR THE TWO-DOF PNEUMATICALLY POWERED WRIST PROSTHESIS.

Requirements	**Target specifications**	
	Quantity	*Unit*
Circumference of a human wrist	165.9 ± 7.10	mm
Maximum mass	< 100	gram
Range of motion for flexion/extension	40/40	°
Range of motion for pro-/supination	50/50	°
Required torque for flexion/extension	300	N·mm
Required torque for pro-/supination	200	N·mm
Minimum locking torque flexion/extension	300	N·mm
Minimum locking torque pro-/supination	200	N·mm
Non-parametric requirements		
No sharp edges and/or pollutants	Simultaneous DoF control	
Provide realistically looking cover	Instantaneous response	
No temperature fluctuations affecting the fitting	No sacrifice of human functional ability	
Independent DoF control	Fluent movements	

3.2 PARAMETER OPTIMIZATION

As was discussed in *2 Background*, gas consumption is one of the main concerns for a pneumatically powered prosthesis. The following subsections will provide a detailed description of the optimization process that fundamentally shaped the parameters of the mechanical design.

First of all, though, every possibility for realizing rotation with a pneumatic actuator must be considered. Rotation can be achieved by two types of mechanisms; *linkage mechanisms* that convert the linear motion from the cylinder into rotation, and the so called *rotary cylinder systems*. Figure 3 shows just several examples of the numerous linkage systems that were considered for the design of the wrist prosthesis. Although the possibilities seem endless, the majority of linkage mechanisms is inadequate to achieve the required rotational range of 100° for pro-/supination. Moreover, doing so in a plane of which the maximum circumference is fixed at 165.9 ± 7.10 mm. proves to be very problematic.

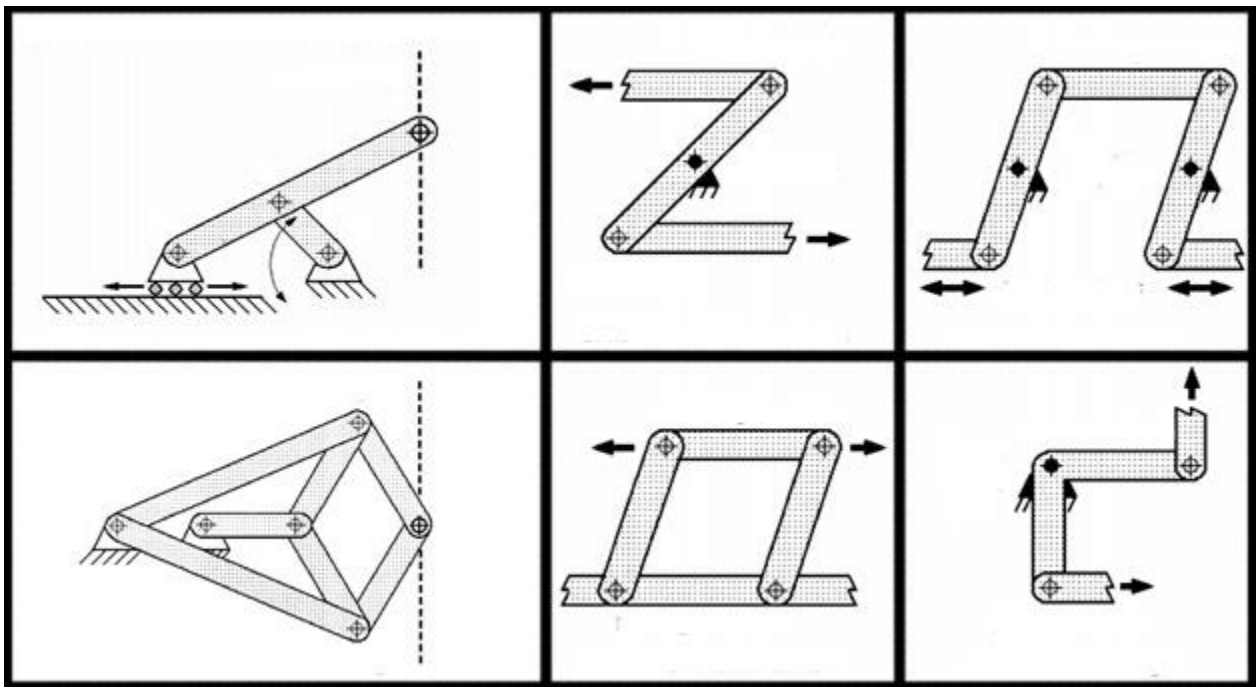

FIGURE 3. EXAMPLES OF LINKAGE MECHANISMS THAT ARE ABLE TO CONVERT THE LINEAR MOTION OF A STANDARD CYLINDER INTO ROTARY MOTION.

The rotary cylinder mechanisms on the other hand are indeed capable of providing the required range of motion within the maximum circumference of a human wrist. On the following page, Figure 4 shows a representation of the most efficient configurations for the four most promising types of rotary cylinders. These cylinder types include;

I. Vane-type cylinder
II. Helical shaft cylinder
III. Single rack cylinder
IV. Double rack cylinder

The ***vane-type cylinder*** (I) works by releasing compressed air on either side of the vane (depicted in black), causing the vane to rotate in the direction where the pressure is lowest. The output torque is a function of the surface area of the vane, and the distance from the middle of that surface area to the center of rotation (i.e. the moment arm). Increasing the moment arm, however, consequently increases the stroke length of the cylinder as well. Parameter

optimization for vane height, vane depth, vane width, moment arm, and stroke length is necessary to determine the optimal configuration.

The ***helical shaft cylinder*** (II) uses the helical shape engraved in the shaft to cause the piston to rotate as it is driven upwards or downwards by pressurized air. The output torque is a function of the cylinder diameter, helical shaft diameter, and the helix angle. A large helix angle is favorable to transmit a high amount of torque, however, increasing the helix angle will simultaneously increase the length of the cylinder (i.e. increase the stroke length) resulting in increased gas consumption. Parameter optimization for cylinder diameter, helical shaft diameter, helix angle, and stroke length is necessary to determine the optimal configuration.

The ***single rack cylinder*** (III) works by having two cylinder heads fastened to the ends of a gear rack. Releasing pressurized air on either side will cause the rack to drive a pinion in the center of the wrist, enabling rotation. The output torque is a function of pinion gear diameter (i.e. the pitch diameter determines the moment arm of the configuration) and cylinder diameter. Increasing the pitch diameter, however, will require an increased length of the gear rack in order to keep the 100° range of motion. This means an increased stroke length resulting in a larger amount of gas consumption. Parameter optimization for pitch diameter, cylinder diameter, and stroke length is necessary to determine the optimal configuration.

The ***double rack cylinder*** (IV) operates very similarly to the single rack cylinder type described above. The addition of another gear rack allows for a more compact configuration which than the single rack cylinder variant. However, the relatively large volume in this particular system that houses the pinion gear is entirely dead space. So although the size of this setup allows for higher output torques than the single rack cylinder in a more compact configuration, the gas consumption to output torque ratio is considerably less favorable. Parameter optimization for pitch diameter, cylinder diameter, dead space, and stroke length is necessary to determine the optimal configuration.

A custom written parameter optimization algorithm using MATLAB® [44] software determined the optimal parameters for each cylinder type to meet the 200 N·mm requirement with which the least amount of gas is consumed. The optimization algorithm revealed that the vane-type cylinder and the single rack cylinder are tied for the two most efficient rotary cylinders in terms of gas consumed per stroke for this particular application. Appendix A shows an overview of the calculations that lay the foundation of this parameter optimization algorithm.

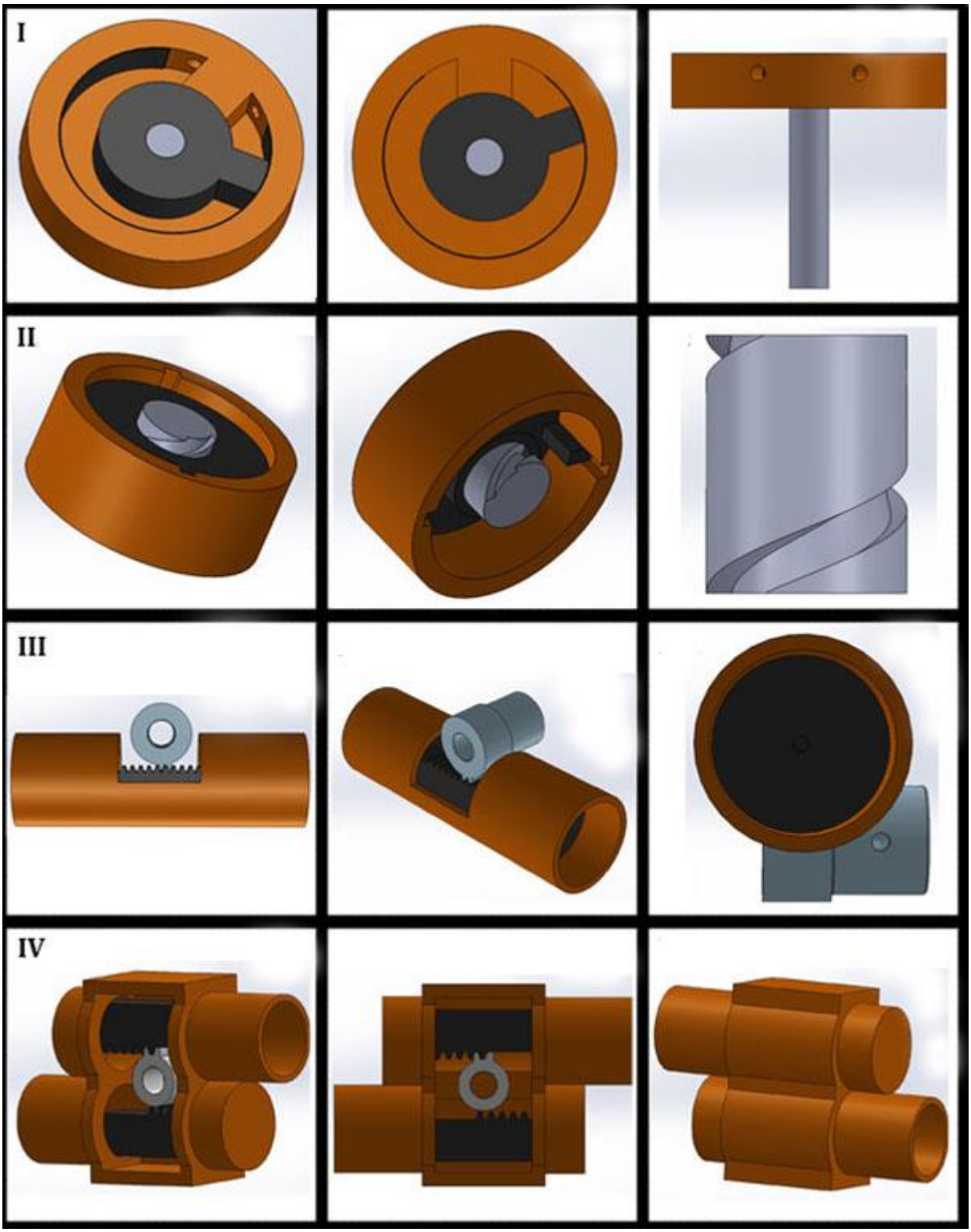

FIGURE 4. DEPICTION OF THE FOUR DIFFERENT ROTARY CYLINDER CONFIGURATIONS MOST SUITABLE FOR PROSTHETIC WRIST DESIGN. THE VANE-TYPE CYLINDER (I) WORKS BY RELEASING COMPRESSED AIR ON EITHER SIDE OF THE VANE (DEPICTED IN BLACK), CAUSING THE VANE TO ROTATE IN THE DIRECTION WHERE THE PRESSURE IS LOWEST. THE HELICAL SHAFT CYLINDER (II) USES THE HELICAL SHAPE ENGRAVED IN THE SHAFT TO CAUSE THE PISTON TO ROTATE AS IT IS DRIVEN UPWARDS OR DOWNWARDS BY PRESSURIZED AIR. BOTH CYLINDER RACK TYPES (III AND IV) WORK BY HAVING CYLINDER HEADS CONNECTED TO A GEAR RACK (DEPICTED IN BLACK). RELEASING PRESSURIZED AIR ON EITHER SIDE WILL CAUSE THE RACK TO DRIVE A PINION IN THE CENTER OF THE WRIST, ENABLING ROTATION.

3.2.1 ROTATION

Considering the fact that both the vane-type cylinder as well as the single rack cylinder are equally efficient, other factors determine the final choice of cylinder type for the prototype of this wrist prosthesis. The single rack cylinder type was chosen to be the most viable option based on the amount of room left for the flexion/extension mechanism and because the exposed pinion gear provides a useful means of simultaneously establishing the wrist locking mechanism.

Simply choosing the parameters that use the least amount of gas does not necessarily mean that this is the absolute best option for the design. There are many other factors in play, such as the dimensions of the flexion/extension mechanism, that may cause the second most efficient option (or third, etc.) to seem more viable for achieving the remaining design requirements.

The full parameter optimization process therefore includes;

1. Calculation of the output torque for every single combination of ***pinion gear diameter*** , and ***cylinder diameter*** and eliminating all options of which the output torque is calculated to be outside the range of 200 – 300 N·mm.
2. Calculation of the resulting length of the cylinder that encompasses the 100° rotational range and eliminating all options that would result in surpassing the 165.9 ± 7.10 mm. wrist circumference requirement.
3. Elimination of all options that include impossibly small pinion gear and/or cylinder diameters.
4. Calculation of the amount of gas used per stroke of the cylinder for the entire 100° rotational range using the ideal gas law.

The resulting gas consumption rates are ranked from least to most after which the ten least gas consuming configurations were listed in a table together with their respective pinion/cylinder dimensions (rounded up the nearest millimeter) as shown in Figure 5. These results stem from a more elaborate form of the calculations shown in *Appendix A – Single Rack Cylinder* to include the compressibility factor for real gas CO_2 properties.

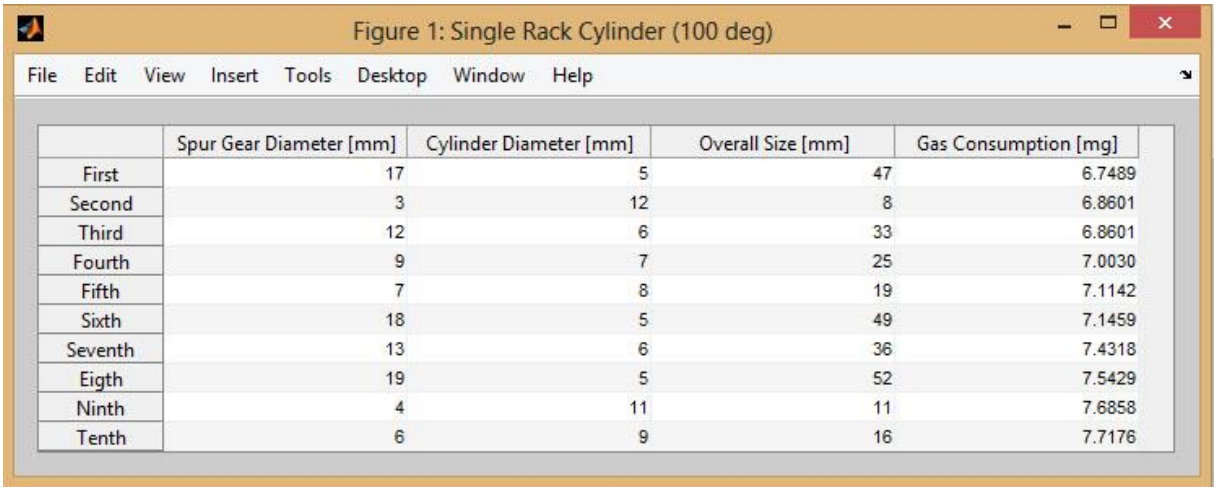

	Spur Gear Diameter [mm]	Cylinder Diameter [mm]	Overall Size [mm]	Gas Consumption [mg]
First	17	5	47	6.7489
Second	3	12	8	6.8601
Third	12	6	33	6.8601
Fourth	9	7	25	7.0030
Fifth	7	8	19	7.1142
Sixth	18	5	49	7.1459
Seventh	13	6	36	7.4318
Eigth	19	5	52	7.5429
Ninth	4	11	11	7.6858
Tenth	6	9	16	7.7176

FIGURE 5. THE RESULTING SET OF CONFIGURATIONS AFTER THE PARAMETER OPTIMIZATION PROCESS. THESE PARAMETERS FOR SPUR GEAR DIAMETER, CYLINDER DIAMETER, AND OVERALL SIZE (I.E. STROKE LENGTH) WILL BE USED AS GUIDELINES TOWARDS THE SUCCESFUL CONJUNCTION OF THE ROTARY CYLINDER, FLEXION/EXTENSION MECHANISM, AND THE LOCKING MECHANISM.

3.2.2 FLEXION/EXTENSION

The mechanism for the second degree of freedom, flexion/extension, does have the opportunity for the installment of a linkage mechanism. It is decided that the most compact configuration consists of a regular lever mechanism of which the actuating cylinder can be installed alongside the rotary cylinder setup. For such a mechanism, there are a variety of parameters that require optimization in order to end up with the least gas consuming configuration. Figure 6 gives a schematic overview of the flexion/extension lever mechanism and it will be used to elaborate on the chosen design parameters in the following subsections.

In Figure 6, the thick lines ***PA***, ***PB*** and ***PC*** represent the lever that serves as the interface to which the prosthetic hand will be attached in its three extremes; -40° flexion, 0° flexion, and +40° flexion. The cylinder rod coming from the cylinder will be coupled somewhere along the length of the hand interface (***x***) to drive the lever from -40° to +40° and vice versa. Coupling the cylinder rod close to the flexion/extension center of rotation (***P***) will ensure a short stroke length to reduce the amount of gas consumed, however, the cylinder diameter will have to be increased accordingly in order to produce an output force adequate enough to provide the 300 N·mm with that chosen moment arm. On the contrary, when a larger distance for ***x*** is chosen, the smaller cylinder diameter will decrease the cylinder volume while the resulting larger stroke length increases the cylinder volume at the same time.

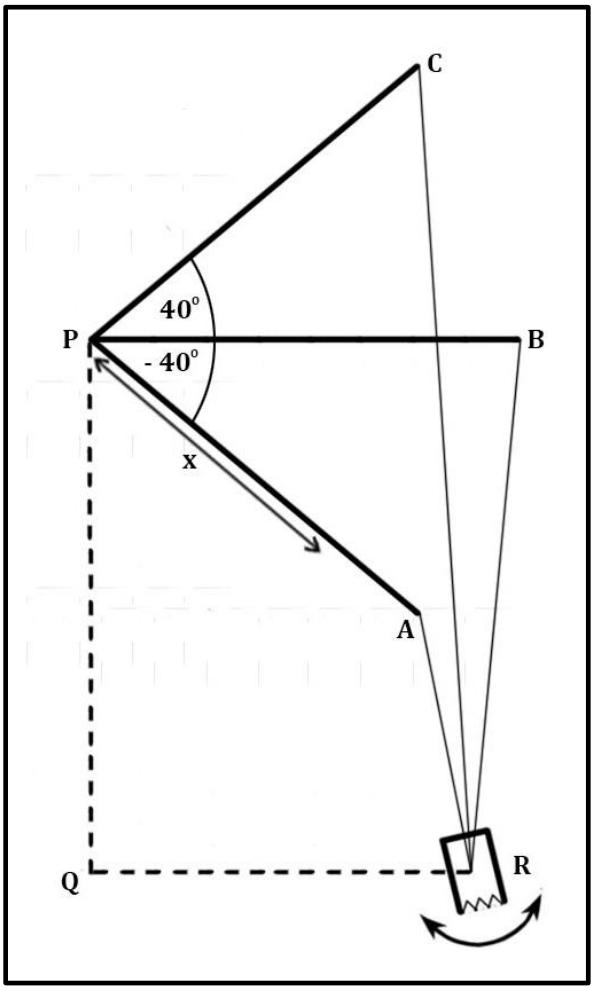

FIGURE 6. SCHEMATIC REPRESENTATION OF THE LEVER MECHANISM THAT WILL BE USED FOR FLEXION/EXTENSION. PA, PB, AND PC REPRESENT THE LEVER TO WHICH THE PROSTHETIC HAND WILL BE ATTACHED IN ITS THREE MOST EXTREME POSITIONS; -40° FLEXION, 0° FLEXION, AND +40° FLEXION. X MARKS THE DISTANCE FROM THE LEVER'S CENTER OF ROTATION TO THE POINT WHERE THE CYLINDER ROD WILL BE CONNECTED. THE DISTANCES QR AND QP REPRESENT THE ORIENTATION OF THE CYLINDER'S CENTER OF ROTATION WITH RESPECT TO THE FLEXION/EXTENSION CENTER OF ROTATION. THESE ARE THE PARAMETERS THAT REQUIRE OPTIMIZATION IN ORDER TO FIND THE CONFIGURATIONS AT WHICH THE GAS EXPENDITURE IS MINIMIZED.

It must be noted that when the prosthetic hand interface moves along its rotational range, the moment arm of the cylinder output force constantly changes. Therefore, the location of the cylinder center of rotation (***R***) plays a vital role in ensuring optimal moment arms over the entire 80° range of motion, and requires optimization of the distances ***PQ*** and ***QR***.

The full parameter optimization therefore includes;

1. Calculation and registration of 81 moment arms (from -40° to +40° flexion) belonging to every possible combination of ***PQ***, ***QR***, and ***x***.
2. Calculation of the output torque for every single moment arm and elimination of the configuration of which one or more of the 81 moment arms proves inadequate to produce the required 300 N·mm.
3. Repeat the process for every possible cylinder diameter.
4. Calculation of the amount of gas used per stroke of the cylinder for the entire 80° rotational range using the ideal gas law.

The resulting gas consumption rates are ranked from least to most after which the ten least gas consuming configurations were listed in a table together with their respective pinion/cylinder dimensions rounded up to the nearest millimeter.

3.3 MATERIALS

The cylinders in the design will be custom machined to ensure that the calculated parameters can be met. These cylinders, cylinder heads, rods, caps, and nozzles will be made from regular carbon steel and sealed off using nitrile butadiene rubber (NBR) O-rings. Any shafts in the system will be machined from regular carbon steel as well on account of its required stiffness properties. The interface that connects the prosthetic hand to the wrist, however, will be made from aluminum in order to save weight. Lastly, the housing of the wrist will be rapid prototyped as much as possible using, acrylonitrile butadiene styrene (ABS) 3D printable plastic on account of its stiffness properties. It must be noted that the materials used in this prototype are not optimized for use in the final product yet (e.g. reducing the overall mass of the wrist prosthesis, reducing cylinder friction, preventing oxidation, etc.). This is considered future work.

3.4 DESIGN

With the fenced off set of configurations for rotation and flexion/extension found in *3.2 Parameter Optimization*, the challenge is to find two configurations (one of each set) that fit together within the given size requirements. The two chosen configurations will be shown in *3.4.1 Rotation* and *3.4.2 Flexion/Extension* after which the locking mechanism is discussed in *3.4.3 Locking Mechanism*.

3.4.1 ROTATION

From the set of configurations for the rotary cylinder, the most compact design was chosen in order to allow room for the flexion/extension cylinder and the locking mechanism to be installed in the same plane. The most appropriate setup in this case proves to be the tenth configuration from the optimization process (Figure 5) as it leaves the largest gap for the rotation of the flexion/extension cylinder (portrayed as ***x*** in Figure 7).

The following design description employs the use of the images shown in Figure 8.

The rotary cylinder consists of two NBR 7x1 mm. O-rings (Ia) that seal off the two pistons (Ib) connected to the round 416 stainless steel rack (Ic) on both sides. The completed assembly (II) is then placed inside the cylinder and sealed off with two cylinder caps (IIIa). A 0.65x0.25 mm. stainless steel nozzle is inserted into the hole in the cylinder cap to allow pressurized CO_2 to be injected in the cylinder chamber (IIIb).

The main rotator shaft is installed perpendicular to the cylinder and kept in place using two ball bearings fitted inside the housing (IIIb). The housing consists of two 3D-printed ABS plastic bodies; the base of the rotator (IVa), and the rotator cover (IVb). These two parts enclose the entire rotator assembly (IVc), including the locking mechanism (discussed in *3.4.3 Locking Mechanism*).

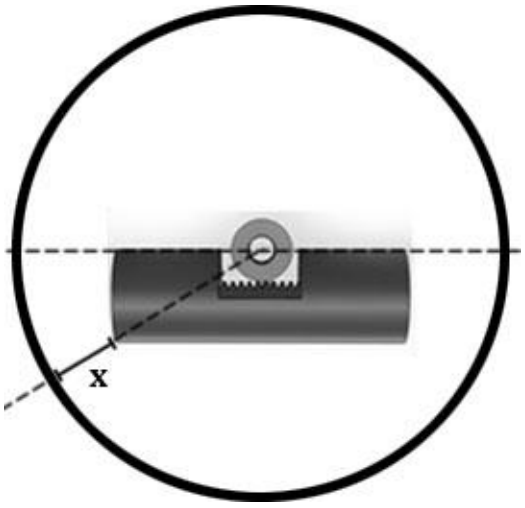

FIGURE 7. SCHEMATIC REPRESENTATION OF THE ORIENTATION OF THE ROTARY CYLINDER IN THE MAXIMUM WRIST DIAMETER. THE FINAL CONFIGURATION IS CHOSEN SUCH THAT THE DISTANCE 'X' IS MAXIMAL IN ORDER TO LEAVE ENOUGH ROOM FOR ROTATION OF THE FLEXION/EXTENSION CYLINDER (AS DISCUSSED IN *3.4.2 FLEXION/EXTENSION*).

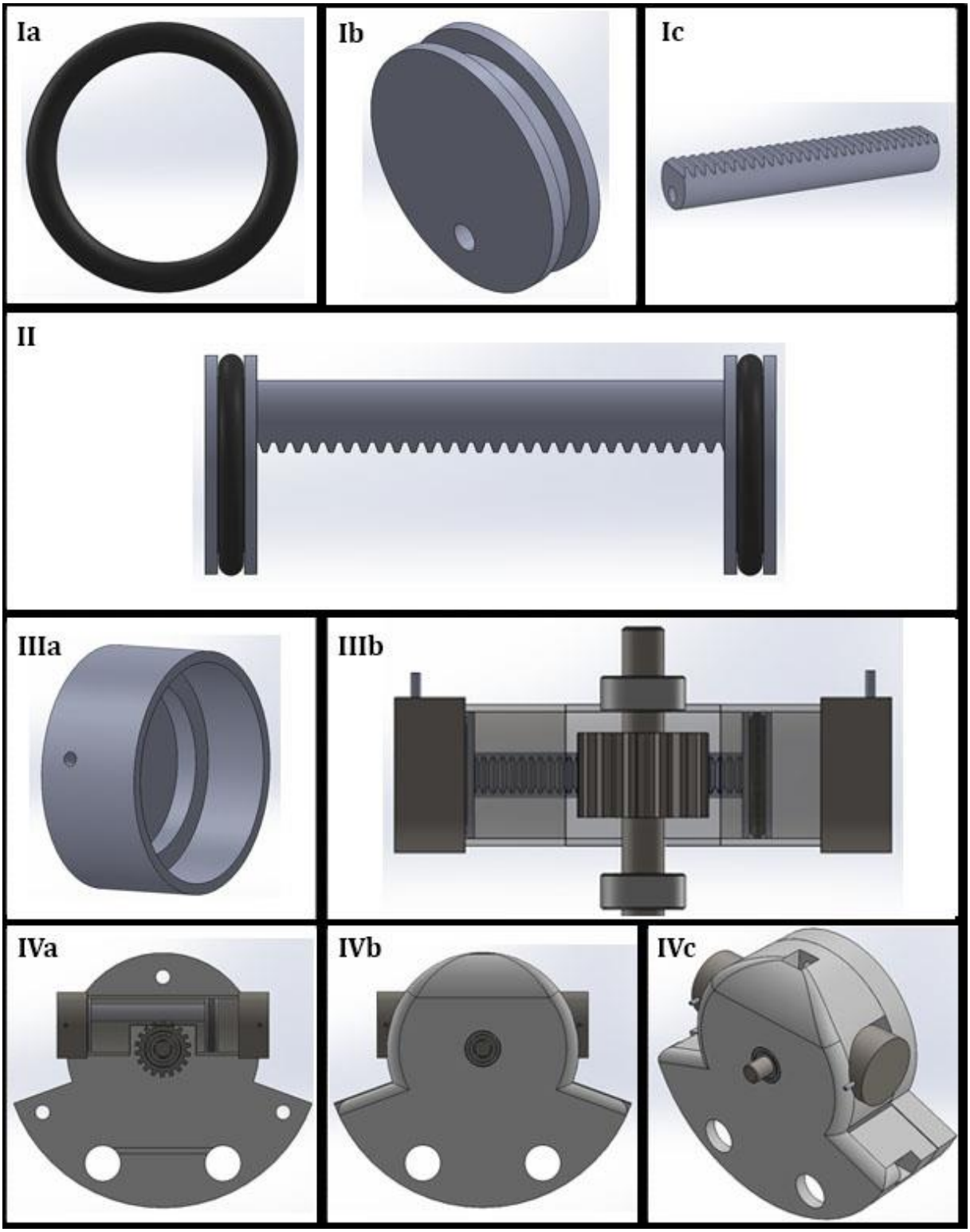

FIGURE 8. (IA) 7X1 NBR O-RING. (IB) CYLINDER PISTON. (IC) ROUND 416 STAINLESS STEEL RACK. (II) ROTARY CYLINDER PISTON ASSEMBLY. (IIIA) CYLINDER CAP. (IIIB) ROTARY CYLINDER ASSEMBLY. (IVA) HOUSING BASE. (IVB) HOUSING COVER. (IVC) FULL ROTATOR ASSEMBLY

3.4.2 FLEXION/EXTENSION

One double acting cylinder is used to bring about flexion/extension in the design. After correcting for the reduced piston surface area the cylinder rod takes up, the optimization algorithm revealed an optimal distance of 24.0 mm. for ***x***, 44.2 mm. for ***PQ***, 23 mm. for ***QR***, and a ***cylinder diameter*** of 5.00 mm (Figure 6).

The following design description employs the use of the images shown in Figure 9.

The 3D-printed ABS plastic housing holds the rotational bearings for both the hand interface and the pivoting double acting cylinder. A digital image of the front view (Ia), and side view (Ib) of the housing is shown. The image Ic shows an exploded view of the double acting cylinder; the cylinder piston is sealed off at the bottom using an NBR 3x1 mm. O-ring while the top is sealed with an NBR 2x1 mm. O-ring for static sealing of the Ø 2 mm. cylinder rod. This upper O-ring is encapsulated between two caps of which the lower cylinder cap contains the hole into which the 0.65x0.25 mm. stainless steel nozzle is placed. The cylinder rod eventually is fitted inside a t-joint that connects to the hand interface.

A front (IIa) and sideview (IIb) of the entire flexion/extension assembly is shown. It can be seen that the aluminum hand interface contains a large M12x1.5 tapped hole in its center which is characteristic for prosthetic hand fittings. In compartments IIIa and IIIb, a bottom view of the complete rotary cylinder and flexion/extension mechanism is shown. This nicely illustrates how the flexion/extension mechanism revolves around the rotary mechanism within the 165.9 ± 7.10 mm. maximum wrist circumference requirement; 0° pro-/supination (IIIa), and ±50° pro-/supination.

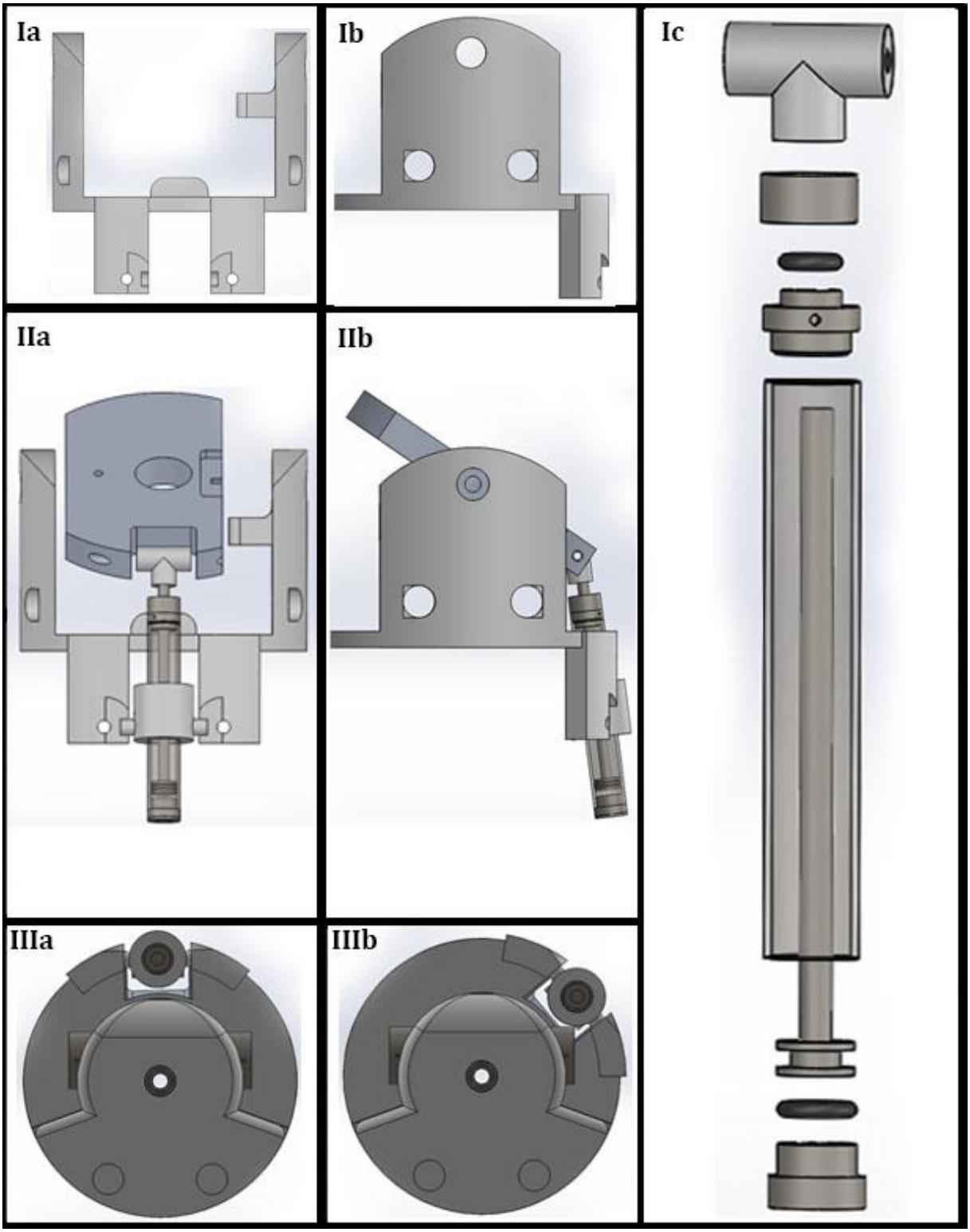

FIGURE 9. (IA) FRONT VIEW OF THE FLEXION/EXTENSION HOUSING. (IB) SIDE VIEW OF THE FLEXION/EXTENSION HOUSING. (IC) EXPLODED VIEW OF THE DOUBLE ACTING CYLINDER. (IIA) FRONT VIEW OF THE ENTIRE FLEXION/EXTENSION ASSEMBLY. (IIB) SIDE VIEW OF THE ENTIRE FLEXION/EXTENSION ASSEMBLY. (IIIA) BOTTOM VIEW OF 0° PRO-/SUPINATION. (IIIB) BOTTOM VIEW OF ±50° PRO-/SUPINATION.

3.4.3 LOCKING MECHANISM

The third major aspect of this design is that after rotation has been realized, the device will have to lock in place. The locking mechanism consists of two pawls that jam the gear rotation in consequence of its wedge-like shape. Two torsion springs (0.45 N·mm/°, max. ∠ 121°) located on each of the pawl's rotational shafts ensure that the pawls are continuously pressed against the teeth of the gear. The location of the these shafts and the pawl's wedge-like contact area ensure that the wrist rotation remains jammed should an external torque be imposed on the hand. For unlocking, a miniature cylinder is installed within the pawl. This cylinder is situated within the same pneumatic circuit as its respective rotational cylinder. This means that when the user initiates rotation, the smaller miniature unlocking cylinder will have filled up sooner than the rotary cylinder, causing the locking mechanism to unlock well before it may obstruct the rotary cylinder's motion. The unlocking cylinder is modeled such that the output torque of the unlocking cylinder is always higher than the torsion spring torque plus the torque caused by gravitational forces on the hand (i.e. the wrist prosthesis will always unlock as long as the prosthetic hand is not subjected to external forces other than the earth's gravitational forces). This characteristic dictates the locking cylinder's diameter (Ø 5 mm. for rotation, Ø 6 mm. for flexion/extension) and its moment arm.

The following design description employs the use of the images shown in Figure 10.

Compartment I shows a bottom view of the inside of the rotary cylinder assembly. For the rotation's locking mechanism, the two pawls are pressed against the pinion gear connected to the cylinder rack. Slots modeled into the pawls allow for the insertion of the miniature cylinders described above. Compartment II shows the locking mechanism for the flexion/extension assembly. Although slightly longer, the locking pawls are identical to those used in the rotary cylinder locking mechanism with grooves modeled into the back of the pawl (IIIa) for insertion of the torsion spring. IIIb shows an exploded view of one of the miniature locking cylinders. The PTFE cylinder head is gradually tapered at the top to allow for a smooth small rotation as the cylinder pushes the opposing pawl slightly outward. An NBR 3x1 mm. and NBR 4x1 mm. O-ring is used to seal off the cylinder head for rotation and flexion/extension respectively. Finally, the spur gear visible in the flexion/extension locking mechanism (II and IIIc) envelopes the hand interface with a tight fit in order to have it rotate in conjunction with the amount of flexion/extension.

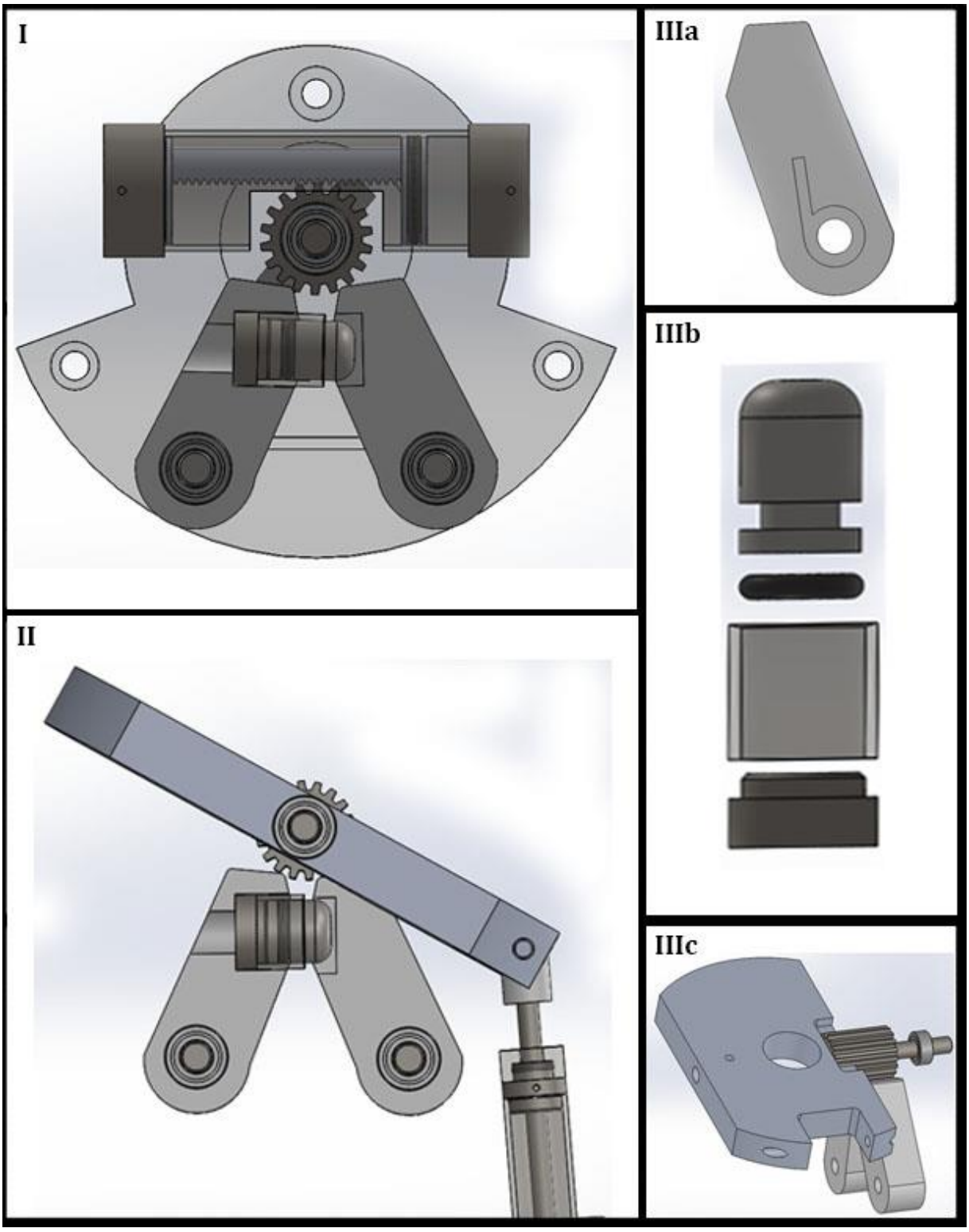

FIGURE 10. (I) BOTTOM VIEW OF THE ROTARY CYLINDER DESIGN INCLUDING THE LOCKING MECHANISM. (II) SIDE VIEW OF THE FLEXION/EXTENSION LOCKING MECHANISM. (IIIA) DEPICTION OF THE BACKSIDE OF ONE OF THE PAWLS USED IN THE LOCKING MECHANISM. THE EXTRUSION FOR THE TORSION SPRING IS CLEARLY VISIBLE. (IIIB) EXPLODED VIEW OF THE MINIATURE UNLOCKING CYLINDER. (IIIC) ISOMETRIC VIEW OF THE FLEXION/EXTENSION LOCKING MECHANISM SHOWING THE CONFIGURATION OF THE LOCKING GEAR ON THE HAND INTERFACE.

3.5 TEST SETUP

The design requirements proposed in *3.1 Design Requirements* are subdivided into parametric and non-parametric requirements. Checking these desired design specifications, such as the maximum amount of output torque, requires some basic experiments to be performed. These tests will reveal the actual values of the six parametric requirements; wrist circumference, total mass, maximum flexion/extension and rotation range of motion, and maximum flexion/extension and rotation output torque.

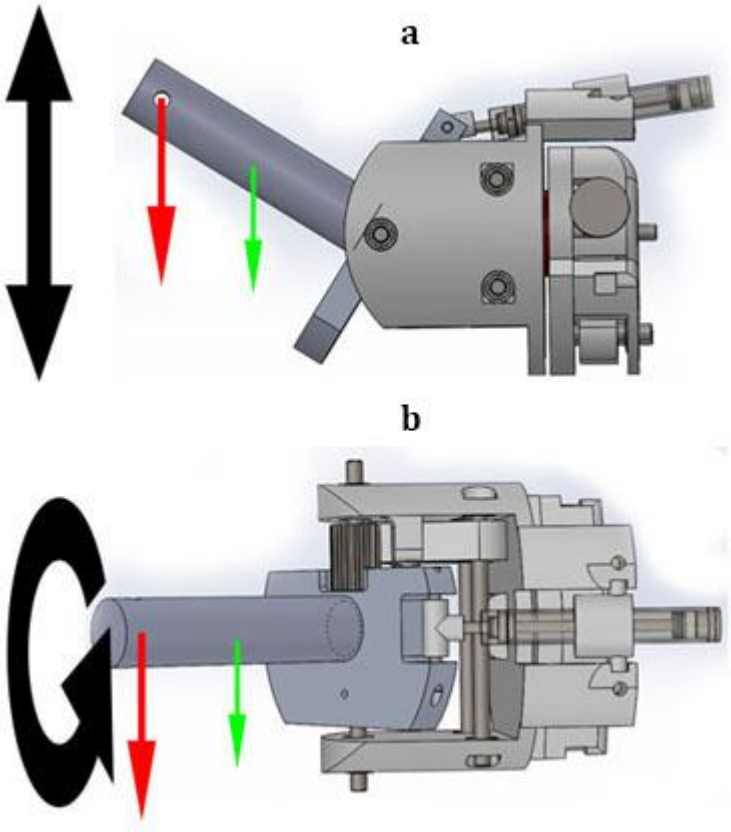

FIGURE 11. SCHEMATIC REPRESENTATION OF THE TEST SETUP FOR MEASURING THE MAXIMUM OUTPUT TORQUE OF THE WRIST PROTOTYPE. THE MAXIMUM OUTPUT TORQUE FOR FLEXION EXTENSION (A) AND ROTATION (B) IS CALCULATED BY ADDING WEIGHTS TO THE END OF THE TESTING ROD (RED ARROW) AND CORRECTING FOR THE GRAVITATIONAL FORCES ACTING ON THE TESTING ROD (GREEN ARROW).

The circumference, total mass, and maximum range of motion are measured by measurement tape, digital scale, and protractor respectively. Measurement of the maximum output torque, however, requires a somewhat more elaborate test setup. A testing rod is placed into the M12x1.5 hole intended for the prosthetic hand. The maximum output torque is calculated by adding weights to the end of the testing rod while increasing the supply pressure to the desired 1.2 MPa. The maximum added weight at which the wrist prototype still operates properly will reveal the maximum output torque. A schematic representation of the test setup is shown in Figure 11.

The maximum allowable torque on the locking mechanism will be determined similarly to the estimation of the maximum output torque. In the same setup as shown in Figure 11, weights will added to the end of the testing rod until the locking mechanism fails or displays angular displacements of the hand interface larger than 10°.

4 TEST RESULTS

The wrist circumference and total mass are measured to be 165.9 (Ø 52.8) mm and 95.4 g respectively. The maximum range of motion for flexion/extension and pro-/supination are 84° and 103° respectively. The test setup described in the previous section revealed that adding 712.2 g to the end of the testing rod (mass 15 g, moment arm 45 mm) for flexion/extension is the limit at which the wrist still operates properly. This comes down to a maximum output torque of 320.9 N·mm for flexion/extension. Unfortunately, the maximum pro-/supination torque capabilities of the prototype remain inconclusive at this point. Inaccuracies in the 3D printed housing are causing an improper fit of the rotary cylinder into the housing. This results in misalignment of the rack and pinion gear combination, causing the rack to slightly rotate within the cylinder and force itself out of contact with the pinion gear. Additionally, local friction peaks on the inner surface of the cylinder were detected when sliding the pistons through the rotary cylinder. Both issues affect the operation of the cylinder such that any measurement taken will not produce representative output torques for its current dimensions.

The flexion/extension locking mechanism reveals that it can withstand a maximum of 797.5 N·mm before it starts to fail (i.e. adding 1.799 kg to the end of the testing rod). The miniature gear rack in the rotary cylinder configuration, however, required the use of a pinion gear with a very large diametral pitch. These miniature gear teeth cause the locking pawls to have an insufficient contact area to latch into, resulting in damage to the ABS plastic pawls to the point where no functional contact area remains. An overview of all design requirements and test results is shown in Table 3.

TABLE 3. OVERVIEW OF ALL THE DESIGN REQUIREMENTS AND ITS CORRESPONDING TEST RESULTS.

Requirements	**Target specifications**	**Measured specifications**	
	Quantity		*Unit*
Circumference of a human wrist	165.9 ± 7.10	165.9 (Ø 52.8)	mm
Maximum mass	< 100	95.4	gram
Range of motion for flexion/extension	40/40	42/42	°
Range of motion for pro-/supination	50/50	51/52	°
Required torque for flexion/extension	300	320.9	N·mm
Required torque for pro-/supination	200	T.B.D.	N·mm
Minimum locking torque flexion/extension	300	797.5	N·mm
Minimum locking torque pro-/supination	200	T.B.D.	N·mm
Non-parametric requirements			
Fluent movements			✓
No sacrifice of human functional ability			✓
No temperature fluctuations affecting the fitting			✓
No sharp edges and/or pollutants			✗
Independent DoF control			✓
Simultaneous DoF control			✓
Instantaneous response			✓
Provide realistically looking cover			✗

5 DISCUSSION AND CONCLUSION

The test results reveal that the optimization process has indeed provided a configuration able to fit two degrees of freedom and a locking mechanism within the confined space of an average human wrist, while being able to generate over 300 N·mm of torque required to flex and extend a 500 g prosthetic hand. However, the test results for the maximum rotational torque remain inconclusive. As described in *4 Test Results*, this is due to the fact that inaccuracies in the 3D printed parts are causing misalignments in the rack and pinion gear combination. A custom machined aluminium housing with the appropriate tolerances should take care of the misalignment issues. Considering the fact that the same optimization algorithm was used for the rotary cylinder as the successful flexion/extension mechanism, it is expected that the parameters of the rotary cylinder are estimated correctly and will not require to be altered in future modifications. The locking mechanism revealed an inconsistency between the flexion/extension mechanism and the rotary cylinder as well. The diametral pitch of the flexion/extension locking mechanism shows it to work perfectly in terms of having the pawls latch firmly into the spur gear, whereas the much larger diametral pitch of the rotary spur gear does not allow a large enough contact area for the pawls (in its current form) to latch into. It must be noted that the size, shape, and torsion springs are dimensioned similarly to the flexion/extension mechanism and that all locking pawls are rapid prototyped with the same 3D printed ABS plastic. In the final product, stainless steel locking pawls should be installed with a custom manufactured interface between the pawl and the spur/pinion gear. This will not only ensure adequate locking for both degrees of freedom, but it will significantly increase the amount of torque the locking mechanism will be able to withstand as well.

Furthermore, the weight of 95.4 grams may further be reduced by choosing more appropriate materials, optimizing shaft diameters, and wall thicknesses to this specific application. Also, finalizing the product beyond the current prototype state will involve completion of the final two nonparametric design requirements; development of a realistic cover and smoothening the entire design into a seemingly edge-free final product.

An important assumption during the development of this prototype is that all the parameters are optimized in order to manipulate a 500 gram prosthetic hand with a center of mass equivalent to a human hand. However, the maximum weight guideline of 500 grams proposed by research groups over the past decades is still very much disputed in literature. Other guidelines include a maximum weight of 400 g [45] or 370 g (including the cosmetic glove) [46]. Either way, the future of upper extremity prosthetics will be themed towards the realization of the much sought-after weight reductions in prosthetic hands. This means that the wrist prototype in its current form may in the future also be used to manipulate small objects should a hand prosthesis be attached that weighs less than the currently assumed 500 grams. Or similarly, the wrist prototype may significantly decrease in size and weight as all wrist dimensions are inextricably blended with the required cylinder diameters.

The assumption of designing the wrist prosthesis for a 500 gram prosthetic hand with a center of mass equivalent to a human hand has led to the optimization of the rotation and flexion/extension cylinders such that an estimated 7.72 mg. CO_2 and 11.37 mg. CO_2 are used per stroke respectively. This comes down to an estimated power supply of 1036 strokes for rotation or 703 strokes for flexion/extension for an 8 gram pressurized CO_2 container. At this point, another optimization step can be performed that possibly further increases the number of strokes before having to replace the empty CO_2 container. As described in *2 Background*, the optimal supply pressure is estimated to be 1.2 MPa based on the analysis of a real gas duct-cylinder system with frictional flow. Although very accurate under normal working conditions, the proposed optimal supply pressure in this analysis does not take into account the system

state at which the pressure in the CO_2 container reaches and surpasses the 1.2 MPa threshold. At this point, the system will no longer be able to perform up to its design specifications and the CO_2 canister requires to be replaced. This means that for a standard commercial 5.7 MPa CO_2 canister, 21% of the CO_2 it contains is redundant and inadvertently disposed of. A more elaborate optimal supply pressure analysis may reveal that although the lower supply pressure operates with less efficiency, it ultimately results in an increase of maximum cylinder strokes due to better use of the available CO_2 per canister.

Other future work includes the development of an adequate control mechanism and the installment of a custom made miniature pressure regulator to allow proportional control of the wrist. This is partly dependent on the manner in which the prosthesis is controlled by the user (e.g. peripheral neural signals, motor cortex signals, EMG mode switching, EMG pattern recognition, etc.), and partly dependent on how the gas supply is stored and whether or not an optimal control algorithm requires the use of separate CO_2 containers per DoF. In the future, for example, custom made CO_2 containers specifically designed to integrate seamlessly into the socket of an upper extremity prosthesis may multiply the amount of gas available in a single container. This brings up the ease and speed at which the CO_2 containers can be replaced to ensure maximum user friendliness. Much rather than replacing the containers (as one would replace an empty battery), it would be much faster and simpler to install a one-way flow check valve into an integrated CO_2 container such that the user can refill the container instantly from a voluminous pressurized CO_2 tank.

Conclusion: *A 95.4 gram pneumatically powered two-degree-of-freedom wrist prosthesis has been developed that enables 42°/42° of flexion/extension and 51°/52° of pro-/supination. The flexion extension actuator provides 320.9 N·mm at 1.2 MPa which is enough to employ a 500 g prosthetic hand for the wrists entire range of motion. A locking mechanism withstanding 797.5 N·mm for flexion/extension is installed to keep the hand locked in position. The lacking test results for the output torque and locking capabilities of the rotator are believed to be solved when the ABS plastic housing and pawls are replaced with aluminium and stainless steel parts respectively. Apart from a custom designed interface between the pawl and the pinion gear, further fundamental changes in the rotator design are not considered a necessity. Although much progress is yet to be made in the aesthetics of the prototype and the development of an adequate proportional control and gas supply system, the fundamental idea of pneumatically powered upper extremity prostheses possess many opportunities in adding more degrees of freedom while still complying with the demand for large weight reductions in upper extremity prosthetics.*

REFERENCES

[1] NLLIC, "Amputation statistics by cause, limb loss in the United States," Amputee Coalition of America, Knoxville, TN, 2008.

[2] J. Pillet and A. Didierjean-Pillet, "Aesthetic hand prosthesis: gadget or therapy? Presentation of a new classification," *Journal of Hand Surgery,* vol. 26B, no. 6, pp. 523-528, 2001.

[3] D. M. Desmond, "Coping, affective distress, and psychosocial adjustment among people with traumatic upper limb amputations," *Journal of Psychosomatic Research,* vol. 62, pp. 15-21, 2007.

[4] A. v. Dijk, Terminologie, classificatie, registratie en epidemiologie van defecten aan de bovenste extremiteit, Nijmegen: Bureau PAOG-Heyendael, 2007.

[5] RSL Steeper, *BeBionic 3,* San Antonio, Texas, USA, 2012.

[6] Touch Bionics, *i-Limb ultra,* Livingston, United Kingdom, 2011.

[7] Otto Bock, *Michaelangelo Hand,* Duderstadt, Germany, 2011.

[8] D. H. Plettenburg, "Basic requirements for upper extremity prostheses: the WILMER approach," *Proceedings of the 20th Annual International Conference of the IEEE Engineering in Medicine and Biology Society,* vol. 20, no. 5, pp. 2276-2281, 1998.

[9] K. Østlie, I. M. Lesjø, R. J. Franklin, B. Garfelt, O. H. Skjeldal and P. Magnus, "Prosthesis rejection in acquired major upper-limb amputees: a population-based survey," *Disability and Rehabilitation Assistive Technology,* vol. 7, no. 4, pp. 294-303, 2012.

[10] B. Peerdeman, D. Boere, H. Witteveen, R. H. i. '. Veld, H. Hermens, S. Stramigioli, H. Rietman, P. Veltink and S. Misra, "Myoelectric forearm prostheses: State of the art from a user-centered perspective," *Journal of Rehabilitation Research & Development,* vol. 48, no. 6, pp. 719-738, 2011.

[11] A. E. Schultz and T. A. Kuiken, "Neural interfaces for control of upper limb prostheses: the state of the art and future possibilities," *The Journal of Injury Function and Rehabilitation,* vol. 3, no. 1, pp. 55-67, 2011.

[12] W. M. Grill, S. E. Norman and R. V. Bellamkonda, "Implanted Neural Interfaces: Biochallenges and Engineered Solutions," *Annual Review of Biomedical Engineering,* vol. 11, pp. 1-24, 2009.

[13] L. F. Nicolas-Alonso and J. Gomez-Gil, "Brain Computer Interfaces, a Review," *Sensors,* vol. 12, no. 2, pp. 1211-1279, 2012.

[14] C. L. Pulliam, J. M. Lambrecht and R. F. Kirsch, "Electromyogram-based neural network control of transhumeral prostheses," *Journal of Rehabilitation Research and Development,* vol. 48, no. 6, pp. 739-754, 2011.

[15] E. Biddiss, D. Beaton and T. Chau, "Consumer design priorities for upper limb prosthetics," *Disability and Rehabilitation: Assistive Technology,* vol. 2, no. 6, pp. 346-357, 2007.

[16] K. Østlie, R. J. Franklin, O. H. Skjeldal, A. Skrondal en P. Magnus, „Musculotskeletal pain and overuse syndromes in adult acquired major upper-limb amputees," *Archives of Physical Medicine and Rehabilitation,* vol. 92, pp. 1967-1973, 2011.

[17] S. L. Carey, M. J. Highsmith, M. E. Maitland en R. V. Dubey, „Compensatory movements of transradial prosthesis users during common tasks," *Clinical Biomechanics,* vol. 23, pp. 1123-1135, 2008.

[18] J. A. Doeringer en N. Hogan, „Performance of above elbow body-powered prostheses in visually guided unconstrained motion tasks," *IEEE Transactions on Biomedical Engineering,* vol. 42, nr. 6, pp. 621-631, 1995.

[19] A. J. Metzger, A. W. Dromerick, R. J. Holley en P. S. Lum, „Characterization of compensatory trunk movements during prosthetic upper limb reaching tasks," *Archives of Physical Medicine and Rehabilitation,* vol. 93, pp. 2029-2034, 2012.

[20] J. S. Landry en E. N. Biden, „Optimal fixed wrist alignment for below-elbow, powered, prosthetic hands," in *Proceedings of the 2002 MyoElectric Controls/Powered Prosthetics Symposium*, New Brunswick, Canada, 2002.

[21] LTI/Liberating Technologies, inc., *VASI Wrist Rotator,* Holliston, MA.

[22] Motion Control, inc., *MC Wrist Rotator,* Salt Lake City, UT.

[23] Otto Bock HealthCare GmbH, *Electric Wrist Rotator 10S17,* Duderstadt, Germany.

[24] P. J. Kyberd, E. D. Lemaire, E. Scheme, C. MacPhail, L. Goudreau, G. Bush en M. Brookeshaw, „Two-degree-of-freedom powered prosthetic wrist," *Journal of Rehabilitation Research & Development,* vol. 48, nr. 6, pp. 609-618, 2011.

[25] K. J. D. Laurentis en S. L. Phillips, „Design of a powered two-DOF prosthetic wrist," in *12th World Congress of the International Society for Prosthetics and Orthotics*, Vancouver, Canada, 2007.

[26] C. Roose, „Multiple-degree-of-freedom powered prosthetic wrist design considerations," Delft University of Technology, Delft, The Netherlands, 2013.

[27] A. E. Kobrinskii, S. V. Bolkhoivin, L. M. Voskoboinikova, D. M. Joffe, E. P. Polyan, Y. L. Slavictskü, A. Y. Sysin and Y. S. Yakobsen, "Problems of bioelectric control," in *Proceedings of the International Federation of Automatic Control Conference*, Moscow, 1960.

[28] D. H. Plettenburg, Upper extremity prosthetics, Delft: VSSD, 2006.

[29] W. Dahlheim, "Pressluft hand für kreigsbeschädigte Industriearbeiter Z. komprimierte und flüssige Gase". Germany 1915.

[30] D. S. Childress, „Historical aspects of powered limb prostheses," *Clinical Prosthetics & Orthotics,* vol. 9, nr. 1, pp. 2-13, 1985.

[31] National Institute of Standards and Technology, "Carbon Dioxide," U.S. Secretary of Commerce, United States of America, 2011.

[32] MOSA, *MOSA CO2 Charger,* Taiwan, Republic of China: MOSA Industrial Corp., 2008.

[33] F. M. White, Fluid Mechanics, 5th Edition, New York, NY: McGraw-Hill, 2003.

[34] D. H. Plettenburg, A sizzling hand prosthesis, Delft: Delft University of Technology, 2002.

[35] D. J. Atkins, D. C. Heard and W. H. Donovan, "Epidemiologic overview of individuals with upper-limb loss and their reported research priorities," *Journal of Prosthetics and Orthotics,* vol. 8, no. 1, pp. 2-11, 1996.

[36] T. Xin, "Singapore Anthropometry Project Report," SIM University, Singapore, 2011.

[37] S. Watve, G. Dodd, R. MacDonald and E. R. Stoppard, "Upper limb prosthetic rehabilitation," *Orthopaedics and Trauma,* vol. 25, no. 2, pp. 135-142, 2011.

[38] D. Childress, "Control of limb prostheses, Chapter 6D," in *Atlas of Limb Prosthetics, Surgical, Prosthetic, and Rehabilitation Principles*, St. Louis, MO, Mosby-Year Book, inc., 1992, pp. 175-199.

[39] G. S. Dhillon, "Direct neural sensory feedback and control of a prosthetic arm," *IEEE Transactions on Neural Systems and Rehabilitation Engineering,* vol. 13, no. 4, pp. 467-472, 2005.

[40] J. Y. Ryu, W. P. Cooney, L. J. Askew, K. N. An en E. Y. Chao, „Functional ranges of motion of the wrist joint," *The Journal of Hand Surgery,* vol. 16, nr. 3, pp. 409-419, 1991.

[41] B. F. Morrey, L. J. Askew en E. Y. Chao, „A biomechanical study of normal functional elbow motion," *The Journal of Bone and Joint Surgery,* vol. 63, nr. 6, pp. 872-877, 1981.

[42] J. T. Belter, J. L. Segil, A. M. Dollar and R. F. Weir, "Mechanical design and performance specifications of anthropomorphic prosthetic hands: A review," *Journal of Rehabilitation Research & Development,* vol. 50, no. 5, pp. 599-618, 2013.

[43] Aerospace Medical Research Laboratory, „Investigation of intertial properties of the human body," U.S. Department of Commerce, Springfield, VA, 1975.

[44] MathWorks, inc., *MATLAB,* Natick, MA: MathWorks, inc., 2014.

[45] J. L. Pons, E. Rocon, R. Ceres, D. Reynaerts, B. Saro, S. Levin and W. V. Moorleghem, "The MANUS-HAND, dextrous robotics upper limb prosthesis: mechanical and manipulation aspects," *Autonomous Robots,* vol. 16, no. 2, pp. 143-163, 2004.

[46] H. W. Kay en M. Rakic, „Specifications for electromechanical hands.," in *Proceedings of the 4th International Symposium on the External Control of Human Extremities*, Belgrade, Yugoslavia, 1972.

APPENDIX A

The following subsections provide an overview of the equations that lay the foundation of the parameter optimization algorithm. The variables in the optimization process are allocated to square matrices that contain a magnitude of different values ranging from zero to somewhat beyond what would reasonably be its maximum value (e.g. a cylinder diameter ranging from zero to little over the maximum allowable wrist circumference).

Using element-wise multiplication of the established parameter matrices the maximum torques and its corresponding gas consumption are calculated for every single combination of the parameter values. Thereafter, all combinations with a maximum torque (T_{max}) of over 200 N·mm are selected and sorted from least to most amount of gas consumed per stroke. All cylinder options are assessed using a supply pressure of 12 bar ($p_{supply} = 1.2 \cdot 10^6$ [Pa]) and assuming ideal gas conditions.

VANE CYLINDER

The torque transmitted from the vane to the shaft depends on the surface area of the vane (A_{vane}) and the distance from the center of the vane to the center of the shaft (r) as shown in Figure 12.

$$T_{\max} = p_{\text{supply}} \cdot A_{vane} \cdot r$$

The variable parameters then include the height of the vane (h_{vane}), width of the vane (w_{vane}), and the diameter of the flange (D_{flange}).

$$T_{\max} = p_{\text{supply}} \cdot \left(h_{vane} \circ w_{vane}\right) \circ \left(h_{vane} + D_{flange}\right) \cdot \frac{1}{2}$$

with

$$h_{vane} = \begin{bmatrix} 0.1 & 0.2 & \cdots & 50 \\ 0.1 & 0.2 & \cdots & 50 \\ \vdots & \vdots & \ddots & \vdots \\ 0.1 & 0.2 & \cdots & 50 \end{bmatrix} \cdot 10^{-3} \text{ [m]}, \text{ and } w_{vane} = D_{flange} = h_{vane}{}^{\mathrm{T}} \text{ [m]}$$

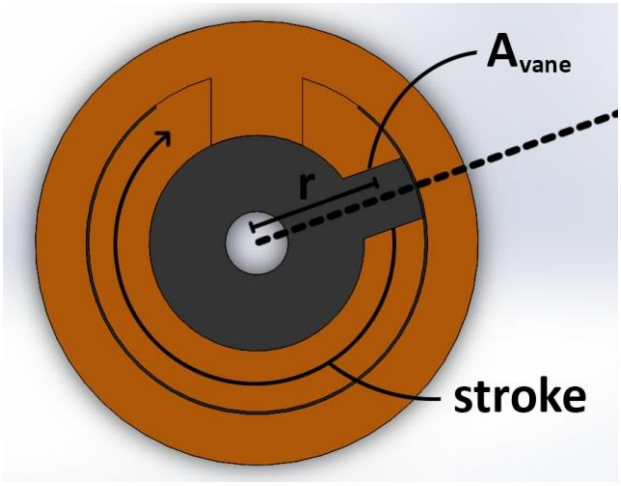

FIGURE 12. SCHEMATIC OVERVIEW OF THE VANE-TYPE ROTARY CYLINDER. THE SURFACE AREA OF THE VANE (A_{VANE}) ALONG WITH THE DISTANCE FROM ITS CENTER TO THE CENTER OF THE SHAFT DETERMINE THE MAXIMUM OUTPUT TORQUE. OPTIMIZATION OF THE HEIGHT OF THE VANE, WIDTH OF THE VANE, AND THE FLANGE DIAMETER IS NECCESARY TO DETERMINE THE OPTIMAL CONFIGURATION.

The amount of gas consumed depends on the volume required for the vane to move from 0° to 100° rotation (i.e. the stroke lenth times the surface area of the vane). The amount of gas consumed per stroke is calculated by

$$CO_2 = \frac{2 \cdot \pi \cdot r \cdot \frac{100}{360} \cdot p_{\text{supply}} \cdot A_{vane} \cdot M_{CO_2}}{R \cdot T} \text{ [kg]}$$

with

$M_{CO_2} = 0.04401$ [kg/mol]

$R = 8.314$ [$m^3 \cdot Pa / mol \cdot K$]

$T = 295$ [K]

HELICAL CYLINDER

The torque transmitted from the cylinder head to the helical shaft is a result of the force generated by the pressure on the cylinder head (F_p). This is a direct result of the effective area of the cylinder head (A_{cyl}) and is determined by the diameter of the cylinder (D_{cyl}) minus the diameter of the helical shaft (D_{helix}).

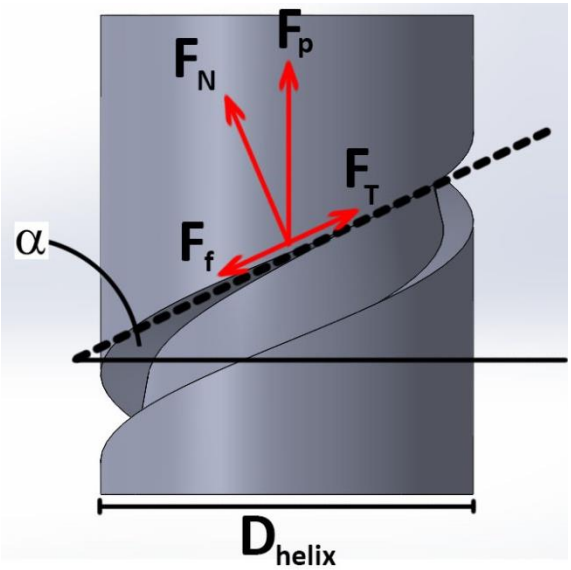

FIGURE 13. THIS FIGURE SHOWS A SCHEMATIC OVERVIEW OF THE DIFFERENT FORCES ACTING ON THE HELICAL SHAFT. CHANGING THE HELIX ANGLE TO ACHIEVE A MORE FAVORABLE OUTPUT TORQUE WILL INCREASE THE STROKE LENGTH, RESULTING IN AN INCREASED AMOUNT OF GAS CONSUMED PER STROKE. OPTIMIZATION OF THE SHAFT DIAMETER, CYLINDER DIAMETER, AND HELIX ANGLE IS NECCESARY TO ENSURE THE MOST EFFICIENT CONFIGURATION.

$$F_p = p_{\text{supply}} \cdot A_{cyl} = p_{\text{supply}} \cdot \frac{\pi}{4}\left(D_{cyl} - D_{helix}\right)^2 \text{ [N]}$$

This pressure generated force (F_p) is transposed into a normal force (F_N) and the force that will ultimately generated the required torque (F_T). After subtraction of the frictional forces (F_f), an estimate can be made on the maximum possible torque (T_{max}). Calculating the maximum torque for every possible configuration requires optimization of D_{helix}, D_{cyl}, and the helix angle (α) as shown in Figure 13.

$$F_T = F_p \circ \sin(\alpha) \text{ [N]}$$

$$F_N = F_p \circ \cos(\alpha) \text{ [N]}$$

$$F_f = \mu \cdot F_N \text{ [N]}$$

A conservative friction coefficient of 0.2 is assumed. The maximum torque can then be estimated by the following equation.

$$T_{\max} = \left(F_T - F_f\right) \circ \frac{D_{helix}}{2} \circ \cos\left(\alpha\right) \text{ [N·m]}$$

with

$$D_{helix} = \begin{bmatrix} 0.1 & 0.2 & \cdots & 50 \\ 0.1 & 0.2 & \cdots & 50 \\ \vdots & \vdots & \ddots & \vdots \\ 0.1 & 0.2 & \cdots & 50 \end{bmatrix} \cdot 10^{-3} \text{ [m]} \qquad D_{cyl} = D_{helix}{}^{\mathrm{T}} \text{ [m]}$$

and

$$\alpha = \begin{bmatrix} 0.2 & 0.4 & \cdots & 100 \\ 0.2 & 0.4 & \cdots & 100 \\ \vdots & \vdots & \ddots & \vdots \\ 0.2 & 0.4 & \cdots & 100 \end{bmatrix} [^o]$$

The amount of gas consumed depends on the volume required for the cylinder to rotate from 0° to 100°. This depends on the diameter of the helical shaft and the helix angle and is calculated by

$$CO_2 = \frac{\mathrm{D}_{helix} \cdot \tan\left(\alpha\right) \cdot \frac{100}{180} \cdot p_{\text{supply}} \cdot A_{cyl} \cdot M_{CO_2}}{R \cdot T} \text{ [kg]}$$

with

$$M_{CO_2} = 0.04401 \text{ [kg/mol]}$$
$$R = 8.314 \text{ [m}^3 \cdot \text{Pa / mol} \cdot \text{K]}$$
$$T = 295 \text{ [K]}$$

SINGLE RACK CYLINDER

The single rack rotary cylinder type bears the most resemblance to a conventional linear cylinder. However, the transfer of the output force from the cylinder head to the spur gear requires an optimization in order to achieve the most gas economical configuration. The maximum output torque can be found with the pressure in the cylinder (p_{supply}) acting on the surface of the cylinder head (A_{cyl}), and the radius of the spur gear (r) as shown in Figure 14.

$$T_{\max} = p_{\text{supply}} \cdot A_{cyl} \cdot r$$

$$T_{\max} = p_{\text{supply}} \cdot \left(\frac{\pi}{4} \cdot D_{cyl} \circ D_{cyl}\right) \circ \frac{D_{spur}}{2}$$

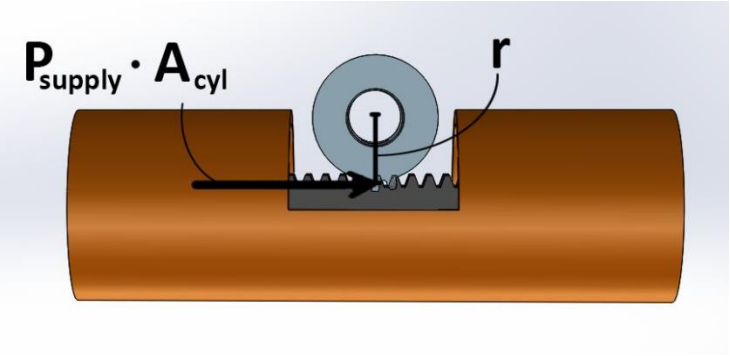

FIGURE 14. SCHEMATIC OVERVIEW OF THE PARAMETERS INFLUENCING THE OUTPUT TORQUE TO GAS CONSUMPTION RATIO.

with

$$D_{spur} = \begin{bmatrix} 0.1 & 0.2 & \cdots & 50 \\ 0.1 & 0.2 & \cdots & 50 \\ \vdots & \vdots & \ddots & \vdots \\ 0.1 & 0.2 & \cdots & 50 \end{bmatrix} \cdot 10^{-3} \text{ [m]}$$

$$D_{cyl} = D_{spur}{}^{\mathrm{T}} \text{ [m]}$$

The gas consumption is then determined with,

$$CO_2 = \frac{\pi \cdot \mathrm{D}_{spur} \cdot \frac{100}{360} \cdot p_{\text{supply}} \cdot A_{cyl} \cdot M_{CO_2}}{R \cdot T} \text{ [kg]}$$

Or, for a real gas $CO_2 = \frac{\pi \cdot \mathrm{D}_{spur} \cdot \frac{100}{360} \cdot p_{\text{supply}} \cdot A_{cyl} \cdot M_{CO_2}}{Z \cdot R \cdot T}$ [kg], with

$Z = 0.94$, corresponding to the compressibility factor for CO_2 at the given supply pressure.

DOUBLE RACK CYLINDER

The output torque for the double rack cylinder is equal to twice the output torque of the double rack cylinder (shown in Figure 15), allowing for smaller cylinder diameters. The stroke length, however, will also be doubled.

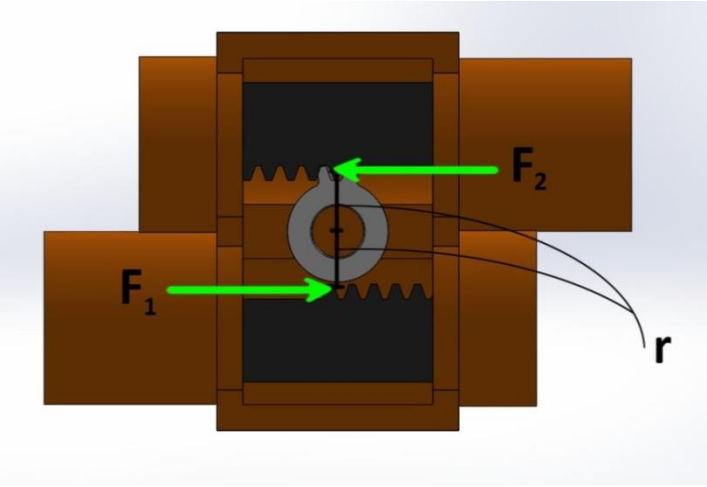

FIGURE 15. SCHEMATIC OVERVIEW OF THE DOUBLE RACK CYLINDER OPTION. THIS DESIGN CAN PRODUCE AN OUTPUT TORQUE IN A MORE COMPACT CONFIGURATION THAN ITS SINGLE RACK COMPETITOR. HOWEVER, THE LARGE AMOUNT OF DEAD SPACE IN THE SPUR GEAR AREA MAKES FOR A SIGNIFICANTLY LARGER GAS CONSUMPTION RATE.

$$T_{\max} = 2 \cdot p_{\text{supply}} \cdot A_{cyl} \cdot r$$

$$T_{\max} = 2 \cdot p_{\text{supply}} \cdot \left(\frac{\pi}{4} \cdot D_{cyl} \circ D_{cyl} \right) \circ \frac{D_{spur}}{2}$$

with

$$D_{spur} = \begin{bmatrix} 0.1 & 0.2 & \cdots & 50 \\ 0.1 & 0.2 & \cdots & 50 \\ \vdots & \vdots & \ddots & \vdots \\ 0.1 & 0.2 & \cdots & 50 \end{bmatrix} \cdot 10^{-3} \text{ [m]}$$

and

$$D_{cyl} = D_{spur}{}^{\mathrm{T}} \text{ [m]}$$

In fact, the ratio of output torque to the amount of gas consumed would be identical to the single rack option were it not for the fact that there is a significant amount of dead space in the area that envelopes the the spur gear. This means that the amount of gas consumed it equal to the single rack option for counter clockwise motion

$$CO_2 = \frac{2 \cdot \pi \cdot \mathrm{D}_{spur} \cdot \frac{100}{360} \cdot p_{\mathrm{supply}} \cdot A_{cyl} \cdot M_{CO_2}}{R \cdot T} \ [\mathrm{kg}]$$

while the amount of gas consumed for clockwise motion is considerably more, as

$$CO_2 = \frac{2 \cdot \pi \cdot \mathrm{D}_{spur} \cdot \frac{100}{360} \cdot p_{\mathrm{supply}} \cdot A_{cyl} \cdot M_{CO_2}}{R \cdot T} + 2 \cdot \mathrm{D}_{cyl}{}^2 \cdot \mathrm{D}_{spur} \ [\mathrm{kg}]$$

SIMULATION RESULTS

The results of the described optimization algorithm are shown in Figure 16 and Figure 17 below.

Figure 1: Vane-type Cylinder (100 deg)

File Edit View Insert Tools Desktop Window Help

	Flange Diameter [mm]	Height of Vane [mm]	Width of Vane [mm]	Gas Consumption [mg]	Torque [Nm]
First	5	7	4	6.3136	0.2016
Second	8	4	7	6.3136	0.2016
Third	17	4	4	6.3136	0.2016
Fourth	3	4	12	6.3136	0.2016
Fifth	4	3	16	6.3136	0.2016
Sixth	5	3	14	6.3136	0.2016
Seventh	6	8	3	6.3136	0.2016
Eigth	8	6	4	6.3136	0.2016
Ninth	9	7	3	6.3136	0.2016
Tenth	10	4	6	6.3136	0.2016

Figure 1: Helical Cylinder (100 deg)

File Edit View Insert Tools Desktop Window Help

	Shaft Diameter [mm]	Cylinder Diameter [mm]	Helix Angle [deg]	Gas Consumption [mg]	Torque [Nm]
First	15	25	30	8.1365	0.2000
Second	42	48	30	8.2016	0.2016
Third	14	24	32	8.2191	0.2016
Fourth	31	38	30	8.2395	0.2026
Fifth	39	45	32	8.2425	0.2022
Sixth	1	40	30	8.2504	0.2028
Seventh	9	22	30	8.2504	0.2028
Eigth	22	30	32	8.2660	0.2027
Ninth	26	34	28	8.3125	0.2028
Tenth	34	41	28	8.3225	0.2030

FIGURE 16.OPTIMIZATION RESULTS FROM THE VANE-TYPE CYLINDER AND HELICAL CYLINDER, SHOWING THE TEN LEAST GAS CONSUMING CONFIGURATIONS.

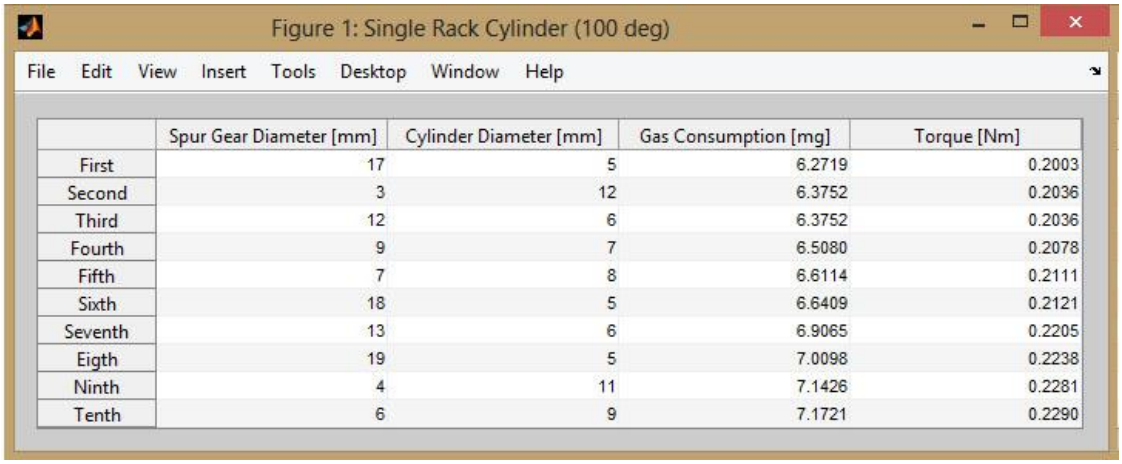

	Spur Gear Diameter [mm]	Cylinder Diameter [mm]	Gas Consumption [mg]	Torque [Nm]
First	17	5	6.2719	0.2003
Second	3	12	6.3752	0.2036
Third	12	6	6.3752	0.2036
Fourth	9	7	6.5080	0.2078
Fifth	7	8	6.6114	0.2111
Sixth	18	5	6.6409	0.2121
Seventh	13	6	6.9065	0.2205
Eigth	19	5	7.0098	0.2238
Ninth	4	11	7.1426	0.2281
Tenth	6	9	7.1721	0.2290

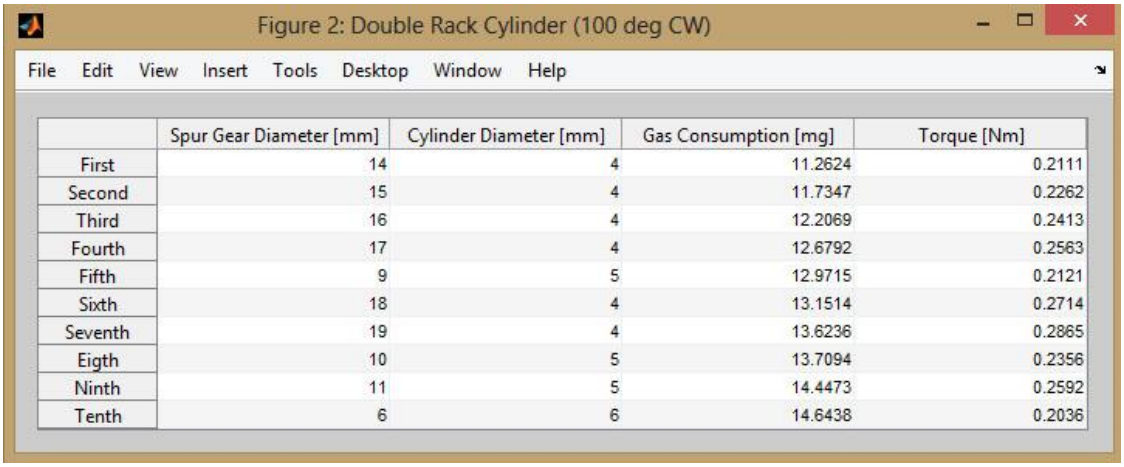

	Spur Gear Diameter [mm]	Cylinder Diameter [mm]	Gas Consumption [mg]	Torque [Nm]
First	14	4	11.2624	0.2111
Second	15	4	11.7347	0.2262
Third	16	4	12.2069	0.2413
Fourth	17	4	12.6792	0.2563
Fifth	9	5	12.9715	0.2121
Sixth	18	4	13.1514	0.2714
Seventh	19	4	13.6236	0.2865
Eigth	10	5	13.7094	0.2356
Ninth	11	5	14.4473	0.2592
Tenth	6	6	14.6438	0.2036

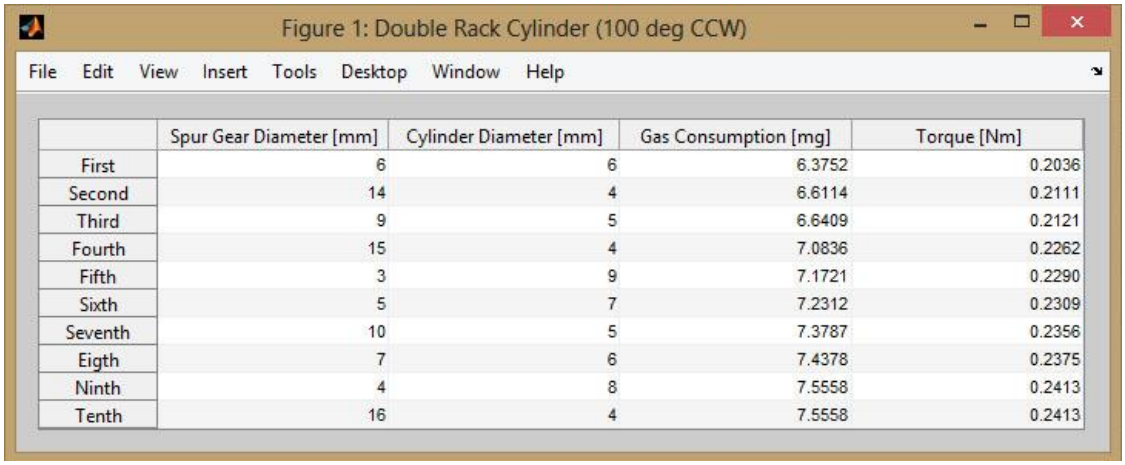

	Spur Gear Diameter [mm]	Cylinder Diameter [mm]	Gas Consumption [mg]	Torque [Nm]
First	6	6	6.3752	0.2036
Second	14	4	6.6114	0.2111
Third	9	5	6.6409	0.2121
Fourth	15	4	7.0836	0.2262
Fifth	3	9	7.1721	0.2290
Sixth	5	7	7.2312	0.2309
Seventh	10	5	7.3787	0.2356
Eigth	7	6	7.4378	0.2375
Ninth	4	8	7.5558	0.2413
Tenth	16	4	7.5558	0.2413

FIGURE 17. OPTIMIZATION RESULTS FROM THE SINGLE RACK AND DOUBLE RACK CYLINDER, SHOWING THE TEN LEAST GAS CONSUMING CONFIGURATIONS. IT CAN BE SEEN THAT THERE IS A CONSIDERABLE DIFFERENCE IN THE CLOCKWISE (CW) AND COUNTER CLOCKWISE (CCW) STROKES FOR THE DOUBLE RACK CYLINDER DUE TO THE AMOUNT OF DEAD SPACE IN THE SPUR GEAR AREA.